Modeling Earth Systems and Environment (2024) 10:3495–3515
https://doi.org/10.1007/s40808-024-01965-w

ORIGINAL ARTICLE

Modeling the environment and climatic conditions of Ladakh Himalaya using Quaternary sediments

Farooq Ahmad Dar[1] · Mamilla Venkateshwarlu[2] · Imran Khan[1] · Malik Zubair Ahmad[3]

Received: 13 November 2023 / Accepted: 19 January 2024 / Published online: 8 March 2024

Abstract

A model of the environmental and climatic conditions in the Ladakh Himalaya is presented by studying the lake sedimentation records preserved in the Shey area of Leh, India. The different layers of the paleolacustrine section were sampled and analyzed for sedimentological, petrological, and magnetic characteristics. The study indicates that a separate lake-damming event, favored by topography, granite bedrock, and moraine and debris material, deposited the 16-m thick sediments. This and similar other past lakes were formed due to the coalescing of southern fan deposits with granite spurs. Locally transported sediments were deposited in three major fluctuating climate and environmental phases. The lower coarser sandy unit represents a fluvial-lacustrine high-energy environment. The middle, thinly laminated clayey unit with uniform characteristics, represents a calm lacustrine and a reducing environment. The topmost 7 m consist of alternating sandy and clayey layers representing an intermittent climate in the catchment. Petrography and magnetic data of the sandy and clayey layers of the section suggest different climates, environments, and mineral assemblages. The average magnetic susceptibility is $\chi = 0.1$ to $< 2.9 \times 10^{-3}$ and 2.9 to 5.7×10^{-3} for the clayey and sandy layers, respectively. Magnetic hysteresis indicates wider loops in clayey layers and thinner loops in sandy layers with saturation fields up to 3000 Oe, whereas thermomagnetic curves show a Curie temperature of 580 °C in most the samples. The hysteresis and K-T curves infer that the clayey layers have a predominance of paramagnetic silicate minerals like haematite, maghemite, ilmenite, goethite, and pyrrhotite and a higher concentration of ferrimagnetic magnetic minerals i.e., magnetite, in the sandy layers. The sandy layers represent a warm and humid climate and a good amount of vegetation cover in the catchment. The sediments were generally transported from variable rock types from the nearby glaciated terrain. The clayey layers represent cooler events. The study indicates that warm and moist conditions occurred at around ca. ~ 100 ka BP that coincided with the intensified Indian Summer Monsoon during the warm interstadial MIS 5c event. The event is attributed to increased glacial melting and intense precipitation in the Ladakh region during the warm interstadial period.

Keywords Lacustrine sediments · Paleo-environment · Rock magnetism · Ladakh Himalaya

Introduction

The Quaternary Period of the Ladakh Himalaya witnessed significant climatic instability (Kumar and Srivastava 2017; Phartiyal et al. 2021; Nag et al. 2023) and intense tectonic disruptions (Kumar et al. 2020; Sharma and Phartiyal 2020). The period also witnessed huge glacial-interglacial fluctuations due to changes in solar insolation and other climatic parameters vis-à-vis global phenomena (Owen 2011). These climatic perturbations caused the failure of the unstable landscapes and triggered huge debris avalanches, extensive fan deposits, and landslides (Kotlia et al. 1997; Nag and Phartiyal 2015; Nag et al. 2016; Lal et al. 2018). The episodic activities at times deposited substantial volumes of sediment at numerous places and blocked and diverted the courses of several rivers, such as the Indus, Shyok, etc., during the Last Glacial Maximum (LGM) (Bhattacharyya 2015; Fort et al. 1989). These blockages created lake conditions in which glacial-fluvial-lacustrine sediments of variable

✉ Farooq Ahmad Dar
farooq.dar1@gmail.com

[1] Department of Geography and Disaster Management, University of Kashmir, Srinagar, India

[2] CSIR-National Geophysical Research Institute, Hyderabad, Telangana 500007, India

[3] Department of Earth Sciences, University of Kashmir, Srinagar, India

characteristics were deposited (Dortch et al. 2011; Sangode et al. 2013; Sharma and Phartiyal 2018). The change in climatic conditions, such as a shift towards warmer conditions, advanced glacial melting, and high precipitation events amplified the volume and energy of water inflow. These factors, coupled with tectonic activities, led to the instability and incision of the blockades and subsequently the draining of the lakes (Phartiyal and Sharma 2009; Phartiyal et al. 2013). The deposits are preserved at many places in the Ladakh region and elsewhere in the Himalayas.

The paleolacustrine deposits provide valuable proxies to reconstruct past processes such as the mechanism of lake formation, phases of sediment deposition, breaching of the dams, and preservation of the remnant sediments, as well as to reconstruct environmental and climatic oscillations. The significance of the sediments has attracted researchers to reconstruct the past meteorological variations, hydrology regimes, tectonic disturbances, sediment transfer processes, and past natural hazards (Mayewski and Jeschke 1979; Owen et al. 1998; Bookhagen et al. 2005; Sangode et al. 2011; Srivastava et al. 2013; Sharma and Phartiyal 2018) as well as in the Leh region (Nag et al. 2016; Lal et al. 2018; Mujtaba et al. 2018; Sharma and Phartiyal 2018).

In the Ladakh Himalayas, the paleolacustrine sediments are preserved at more than seven locations in the 40-km stretch of the Leh valley between Karu (Rambirpura) in the south and the confluence of the Zanskar River in the northwest. Outside the valley, more than 12 identified sections show vast diversity in their distribution and characteristics (Table 1 and Fig. 1). The sediments are preserved as patches or thick valley-fill deposits and are pure clay to silt–clay in composition and interbedded with glacial and/or alluvial sediments. The sediment thickness varies from < 2 m (m) to more than 68 m. The majority of the deposits have been washed away by subsequent erosion and are incomplete in sequence, making their correlation difficult (Huang et al. 2020). Some are hidden under recent alluvium, while others remain unexplored in complex topography.

The governing processes mostly remain questionable and demand further studies. Few workers suggest a single major extensive phase of lake formation occurred in the Indus Valley (e.g., Blöthe et al. 2014), while others propose two separate lakes, the Zinchen-Shey and the Spituk (Mujtaba et al. 2018). Furthermore, the sediments have been dated using multiple chronological techniques such as 10Be Terrestrial Cosmogenic Nuclide, Optically Stimulated Luminescence, and Radiocarbon Dating (e.g. Sharma and Chand 2016). However, the timing of the deposition remains discrepant while using multiple approaches at the same site in the region (Dortch et al. 2009; Sharma and Phartiyal 2018; Shukla et al. 2020; Jena et al. 2022). In addition, the correlation of the fragmentally preserved sections also makes chronologies even more ambiguous (Phartiyal et al. 2022). The present study aims to reduce this knowledge gap by using sedimentologic, petrographic, and magnetic approaches to reduce this ambiguity in dating and modelling such processes. The present near-continuous paleolacustrine section of the Ladakh region represents one of the ideal sections for understanding the past environmental and climatic conditions in the Ladakh.

Study area

The Leh Valley is an arcuate depression in the Ladakh Trans-Himalayan region along the northeast to southwest flowing Indus River between 31° 10′ to 31° 40′ N Lat. and 78° 05′ to 78° 45′ E Long (Sant et al. 2011a, b). It is about 50 km long and 0.5 to 2 km wide, located between Rambirpur in the northeast and Zinchan (the confluence of the Rumbak River) in the southwest, with a meandering and braided flow at places (Fig. 1a). The valley has an irregularly embayed right (northern) bank and a well-defined left (southern) bank with a sharp scarp of about 25 m height near Spituk (Patel et al. 2022). The Indus, which flows for a length of ~ 422 km in India, is an important river in Ladakh that has played a vital role in shaping the topography of the region (Kumar and Srivastava 2018).

Ladakh presently has a cold, arid to semi-arid climate (Juyal 2014). Leh is a rain shadow area between the southern Great Himalayas and the northern Karakoram Range. It receives scanty and infrequent rainfall and snowfall, mainly due to the mid-latitude Westerlies (MLW) and the Indian Summer Monsoon, or ISM (Owen and Benn 2005; Bhutiyani et al. 2010; Arora et al. 2023). The climate is affected due to the shifting of the Intertropical Convergence Zone (ITCZ) towards the north or south (Kumar et al. 2022). When the ITCZ was further south during different climate stages, like during Marine Isotope Stage-2 (MIS) (Jena et al. 2022), the area recieved more rain from the MLW and ISM. The region has sparse vegetation, which consists of xerophytic plants, shrubs, and small trees and is characterised by denuded barren mountain slopes.

The geology of the Leh intermontane valley is characterised by marine-to-continental origin lithotectonic units (e.g., Garzanti and Van Haver 1988; Searle et al. 1990; Sinclair & Jaffey 2001; Clift 2002; Petterson 2023). Towards the north is the Ladakh range, composed of an undeformed Batholith of nearly 102–60 Ma age (Scharer et al. 1984; Upadhyay et al. 2008). The granite body is intruded by dykes as young as c. 45 Ma (Heri et al. 2015). The northern part of the batholith has Khardung Volcanics that represent remnants of past volcanic activity (e.g., Lakhan and Singh 2019). Ladakh Range has uplifted during the late Eocene with differing rates in different parts (Zhou et al. 2020). The southern region includes the folded and thrusted Zanskar Range of the

Table 1 Details of the palaeolacustrine sediments preserved in the Leh Valley and nearby areas of Ladakh Himalayas

Leh valley	Section	Lat. N	Long. E	Time period	Duration	Environment	Proxy	References
Spituk	Lacus	34° 7′ 52″	77° 31′ 43″	177–72 ka	102 ka	F-L	OSL/10Be	Blöthe et al. (2014)
Spituk	Lacus	34° 7′ 52″	77° 31′ 43″	50–30 ka BP (inverse ages)	20 ka	F-L	Radiocarbon	Phartiyal et al. (2005) and Phartiyal et al. (2011)
Spituk	Lacus	34° 7′ 52″	77° 31′ 43″	35–18 ka BP	17 ka	F-L	Radiocarbon	Phartiyal and Sharma (2009)
Spituk	Alluv. Fan	34° 7′ 52″	77° 31′ 43″	78.8 ka	–	Fluvial	OSL	Mujtaba et al. (2018)
Spituk	Lacus	34° 7′ 52″	77° 31′ 43″	78.8–46.7 ka	32.1 ka	F-L	OSL	Lal et al. (2018) and Mujtaba et al. (2018)
Spituk	Lacus	34° 7′ 52″	77° 31′ 43″	> 72—< 32 (top units)	> 32 ka	F-L	OSL	Sangode et al. (2013)
Spituk	Lacus	34° 7′ 52″	77° 31′ 43″	10,530–3250 a	7280 a	F-L	14C	Phartiyal et al. (2013) and Achyuthan et al. (2016)
Spituk	Lacus	34° 7′ 52″	77° 31′ 43″	10 ka (base)	–	F-L	OSL	Phartiyal et al. (2013)
Gupuk	Lacus	34.15°	77.5°	5960 a (middle)	–	F-L	14C AMS	Phartiyal et al. (2013)
Phey	Phyang Fan	34° 8′ 2″	77° 27′ 58″	79.4 ka	–	Fluvial	OSL	Mujtaba et al. (2018)
Phey	Lacus	34° 9′ 15″	77° 25′ 50″	124–114 ka	10 ka	F-L	OSL	Mujtaba et al. (2018)
Opp. Phey Village	Lacus	34° 7′ 49″	77° 27′ 28″	87 ka (base)	–	F-L	OSL	Mujtaba et al. (2018)
Sumdo	Lacus	34° 40′ 51″	77° 37′ 58″	80 ka (middle)	–	F-L	OSL	Lal et al. (2018)
Palam	Allu. Fan	34° 6′ 57″	78° 31′ 18″	74 ka	–	Fluvial	OSL	Mujtaba et al. (2018) and Lal et al. (2018)
Shey	Lacus	34° 4´ 33″	77° 38´ 25˝	93–91 ka	2 ka	F-L	OSL	Mujtaba et al. (2018)
Bajada (left bank)	Lacus	34° 9′ 2″	77° 27′ 58″	72 ka	–	F-L	OSL/10Be	Sangode et al. (2013) and Blöthe et al. (2014)
Outside Leh valley								
Kiyari	Lacus	33° 29'	78° 8'	13 ka (top)	–	F-L	14C AMS	Phartiyal et al. (2013)
Nimo	Lacus	34.19°	77.36°	23–21 ka	2 ka	F-L	14C AMS	Phartiyal et al. (2013)
Nimo	Lacus	34.2°	77.36°	387–111 ka & 265–135 ka	–	F-L	14C AMS	Blöthe et al. (2014)
Markha	Lacus	34° 7′ 13″	77° 25′ 15″	125–87 ka (upper units)	38 ka	F-L	OSL	Mujtaba et al. (2018)
Saspol	Lacus	34° 15′	77° 10.94′	10,850 a BP (base)	–	F-L	14C AMS	Nag and Phartiyal (2014)
Nurla	Lacus	34° 18′	77° 01′	7905 a BP (lower)	–	F-L	14C AMS	Nag and Phartiyal (2014)
Rizong	Lacus	34° 26′	77° 7.3′	17–13 ka BP	4 ka	F-L	14C AMS	Phartiyal et al. (2013) and Nag and Phartiyal (2014)

Table 1 (continued)

Leh valley	Section	Lat. N	Long. E	Time period	Duration	Environment	Proxy	References
Khaltsi	Lacus	34° 20′	76° 52.5′	14,600–5000 a BP	9600 a	F-L	14C AMS	Nag and Phartiyal (2014) and Phartiyal et al. (2013)
Khaltsi	Lacus	34° 20′	76° 52.5′	1635 a BP (top)	–	F-L	14C AMS	Nag and Phartiyal (2014)
Achinathang	Lacus	34° 29′	76° 38.9′	10,715–9875 a BP	840 a	F-L	14C AMS	Nag and Phartiyal (2014)
Hanuthang	Lacus	34° 33′	76° 35′	11 ka (lower)	–	F-L	14C AMS	Nag and Phartiyal (2014)
Bhima	Lacus	34° 36'	76° 30.7′	13,930–6080 a BP	7850 a	F-L	14C AMS	Nag and Phartiyal (2014)
Lamayuru	Lacus	34° 16′ 58″	76° 46′ 28″	35–25 ka	10 ka	F-L	OSL and 14C AMS	Fort et al. (1989), Kotlia et al. (1997), Nag and Phartiyal (2014) and Achyuthan et al. (2016)
Lamayuru	Lacus	34° 16′ 58″	76° 46′ 28″	35 ka (base)	–	F-L	Radiocarbon	Phartiyal et al. (2005)
Lamayuru	Lacus	34° 16′ 58″	76° 46′ 28″	35–40 ka (base)	–	F-L	Fossils	Shukla et al. (2002)
Leh Valley	Sand ramp	34° 9′ 37″	77° 32′ 46″	25–17 ka and < 12–8 ka	–	Arid/windy	OSL	Kumar and Srivastava (2017)
Leh Valley	Sand/Clay	34° 9′ 37″	77° 32′ 46″	~ 12 & ~ 7 ka	–	F-L	OSL	Kumar and Srivastava (2017)

F-L Fluvio-lacustrine

early Miocene to late Paleocene age, called the Indus Formation, and the Zanskar meta-sedimentary Formation of the Paleocene to Paleozoic age (Sinclair and Jaffey 2001). The Zanskar Ranges are composed of fossiliferous limestone, shale, and sandstone and overly ophiolitic melanges and molasses of the Cretaceous to Tertiary age (Robertson and Collins 2002). According to Clift (2002), the Indus Tsangpo Suture Zone (ITSZ) largely determines the Indus River's course as it flows along the contact zone of the Batholith and meta-sedimentary rocks. The geological map around the study site shows the present-day river course, granite ridges, and the lake sediment extension (Fig. 1b). There are several preserved paleolake sections in the valley between Karu and Zinchen along the profile of the Indus River, where major alluvial fans are located (Fig. 1c).

The Shey paleolacustrine section is located at Shey village, about 13 km from Leh town along the Leh-Manali Highway (34° 4′ 33.11″ N, 77° 38′ 24.92″ E) at an altitude of ~ 3268 m msl on the right bank of the Indus River (Fig. 1). The sediments are located in a small valley where the Stakma Stream confluences with the Indus River (Fig. 1b). Satellite image and field observations show that the section approximately extends for 0.8 km in length and 200 m in width. The sediments have been eroded to the present extent of less than 0.1 km^2. The topmost level of the section indicates that the rectangular-shaped lake might be of ~ 5 km^2 area at its peak level. The present patch of sediments is further threatened due to construction and anthropogenic activities.

Material and methods

Sedimentology, petrographic and magnetic examinations, and the dating studies were conducted on the 16.5-m-thick paleolacustrine section. The litholog was created using the in-situ grain-size observations of the distinct layers. The thin sections of the selected layers were prepared at Lab Crystals at Lucknow, and the petrographic examination of the microphotographs was performed at the University of Kashmir using a Leica DM750P microscope with an attached camera and LaSEZ software.

10 g of each sample were collected in separate polythene bags for the magnetic investigation using a non-magnetic spoon. Magnetic susceptibility measurements were taken with a Kappa Bridge MFK1-FA susceptibility meter (AGICO, Czech Republic). Researchers have used the magnetic susceptibility of various kinds of sediments

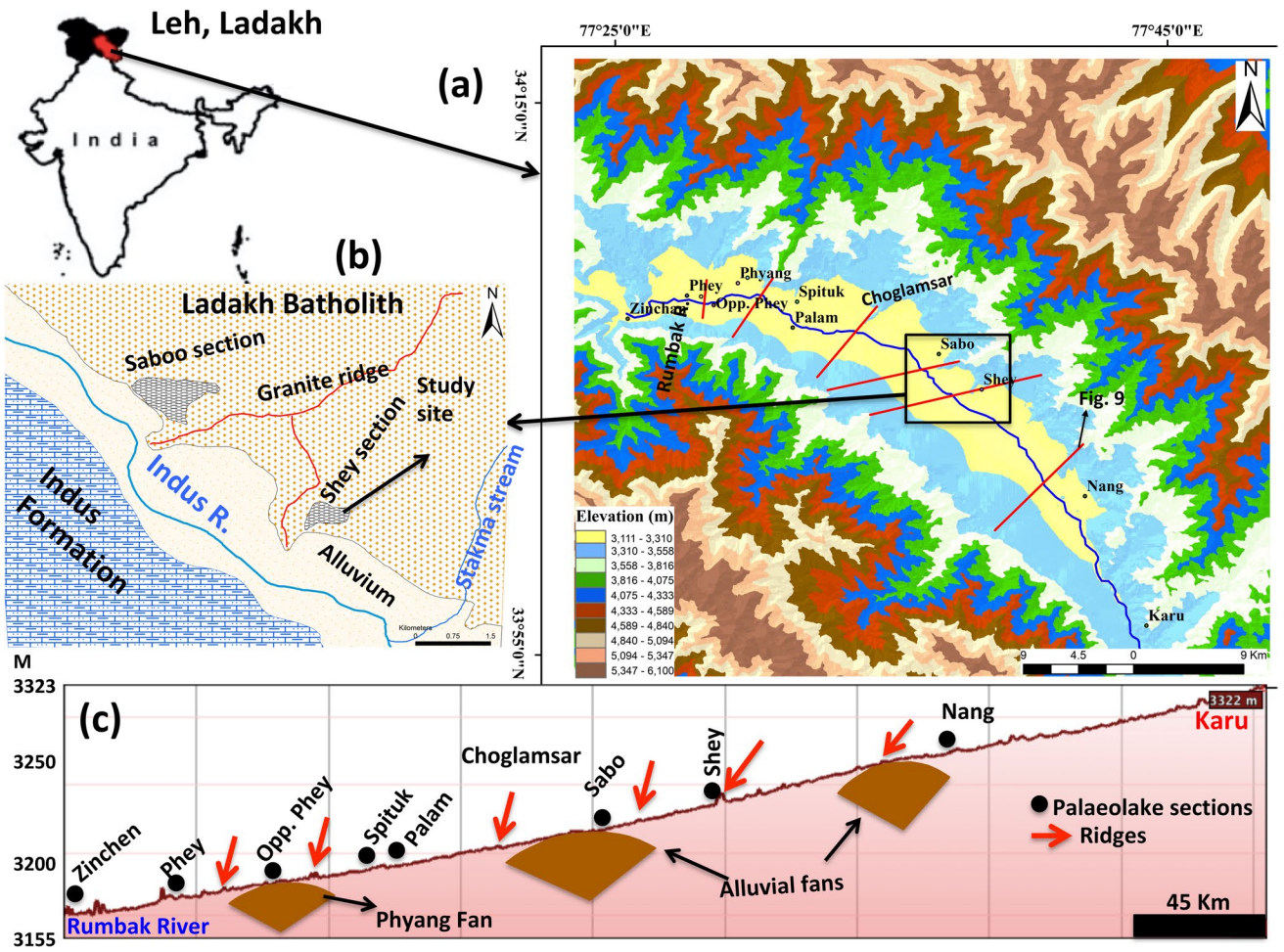

Fig. 1 **a** Location map, showing different lacustrine sediments in Leh, Ladakh. Red lines represent the topographic profiles along the valley as shown in Fig. 9, **b** closer view of the Shey section showing the geomorphic and geologic picture around the site, and **c** topographic profile of Leh valley from upstream to downstream showing the major fan (brown polygons) and ridge elevations along the river course of the major lacustrine sediments

as an environmental proxy (Evans and Heller 2003; Yin et al. 2002; Bhattacharyya et al. 2015). The representative samples weighing 400–600 mg, the magnetic properties, such as susceptibility, hysteresis loops, and thermomagnetic curves were investigated. An advanced variable field translation balance (AVFTB) to determine the magnetic mineralogy, thermomagnetic stability, mineral particle sizes, and domain states of the materials was used. In diverse types of sediments, magnetic hysteresis loops are used to infer crucial parameters such as grain size, mineral content, and so on (Jackson et al. 1989; Lascu and Plank 2013). The hysteresis loop helps in identifying the domain state and the size of the magnetic particles. Thermomagnetic curves (K–T) involve heating the samples to a maximum temperature of 700 °C and again cooling them back to room temperature. The curves allow the identification of the Curie temperature (Tc), the stability of the principal magnetic carriers, and phase change during the heating and cooling process (Wang et al. 2004). Thermomagnetic (K-T) curves have also been used to identify different types of magnetic mineral phases and infer grain size and mineral composition in varied sediment types (Jackson et al. 1989; Dunlop and Ozdemir 1997). The Tc was determined by an intersecting tangent method, which is the maximum gradient in the heating curve. The heating treatment was performed using the MMTD-80 thermal demagnetizer (Magnetic Measurements, UK) and the remanence was measured using AGICO's JR6 spinner magnetometer (Czech Republic). The magnetic measurements were carried out at the Paleomagnetism Laboratory, CSIR-National Geophysical Research Institute (NGRI), Hyderabad, India. The magnetic measurements and data interpretation were done based on the developed methodology (e.g., Dekkers 1997; Vlag et al. 1997; Maher and Thompson 1999; Li et al. 2006; Sangode et al. 2013; Kapawar and Venkateshwarlu 2020; Ahn et al. 2021).

Optically stimulated luminescence (OSL) dating was done on sandy horizons from the section using steel tubes that were 10 inches long and 1.5 inches wide. The middle portion of each tube was processed and cleaned. The dating was performed at the Birbal Sahani Institute of Paleosciences in Lucknow, India, using a Riso TL/OSL DA-20 apparatus and a filtered Sr90 radiation source. In subdued red light, standard procedures were used to remove quartz grains of 90 micron diameter from the samples. Numerous authors (e.g., Rhodes and Bailey 1997; Jaiswal et al. 2008; Phartiyal and Sharma 2009; Rhodes 2011; Nawaz Ali et al. 2013) have examined the ageing methodology. OSL is a widely used method for dating past events and deposits as young as one year to two hundred thousand years (Aitken 1998; Galbraith et al. 1999; Rhodes 2011; Morthekai and Nawaz Ali 2014; Chaudhary 2015). The method has some limitations (Wallinga 2002; Kolstrup 2007) but is also preferred over other dating methods (e.g., Murray and Olley 2002). Table 2 provides the details of the samples, dose rate, and OSL ages obtained in this study.

Results

Lithology of the Shey section

The section is about 16.5 m thick (highest elevation: ~ 3260 msl) and has three sedimentation units (S1, S2, and S3) with visual lithological variations (Fig. 2). Mujtaba et al. (2018) demarcated the three layers, but no detailed discussion is provided about the layer-wise characteristics. The lower S1 unit (Fig. 2) is mostly obscured under the eroded material but is exposed towards the left end of the valley (inset in Fig. 2) due to the ongoing mining activities. The unit comprises mostly fine to coarse sand and overlies the batholith basement. The total thickness of the unit is ~ 4.5 m and has five major layers with color varying from greyish yellow (or 5Y 8/4 as per The Rock Colour Chart Committee 1980) to moderate reddish brown (or 10R 4/6) color.

The middle S2 unit is ~ 5.6 m thick, composed of clay with a minor silt content, and has a moderate yellow colour (or 5Y 7/6) (Fig. 3). The entire unit is a thick bed of laminated clayey sediments with well-preserved laminations ranging in thickness from mm to cm. Except for the folded, undulated, and jointed beddings, there are no sedimentary structures.

The topmost S3 unit is almost 8 m thick with many thin intercalated layers (Fig. 4). There are nine sedimentation cycles in all, each beginning with a coarser (sandy) facies of mild yellowish brown (or 10YR 5/4) and ending with a clayey layer of dusky yellowish brown color (or 10YR 2/2). Five (5) such cycles with intercalated clayey beds are identified in the lower two meters at 11.20 m, 11.48 m, 12.33 m, 13.9 m, and 14.27 m (Fig. 5). The S3 unit begins with a fine to coarse sand bed, which marks an incision surface with the S2 unit (see Fig. 2). Figure 5 depicts the section's lithology, sedimentology, OSL, and the susceptibility values.

Petrography of the sediments

The petrographic analysis indicates that majority of the clay layers of the section have almost a similar mineralogy with a small variation. Figure 6 provides the microscopic picture of the selected clayey layers from the three units (S8, S27, S31, S38, S47, S54). Quartz, muscovite, k-feldspar, and little amphiboles are the major minerals in the layers. Some pyroxenes showing greenish to pinkish pleochroism are identified. Grains are angular to subangular, well sorted, fine-grained, and show porphyritic and porphyroskelistic texture with granostriated fabric. Some biotites are slightly altered. The black, rounded particles are the oolitic structures and fossil shells, which are abundant in quantity. The curved structures are possibly microfossils. Some sections show impregnations of Fe/Mn oxides, chert, and opaque minerals such as sulphides and oxides. Some of the clayey layers, such as S31 and S38 (Fig. 6) show channels with a thin $CaCO_3$ coating and nodules. Minor amounts of staurolite and altered garnet minerals are also seen. The thin sections indicate slightly reworked sediments. Therefore, the major composition of the clayey layers of S1 and S3 units and that of the whole S2 unit are clay minerals with quartz, biotite, feldspars, rock fragments, and chert. The brownish colour and altered boundaries of minerals indicate the high degree of weathering.

The sandy layers of the S1 and S3 units (Fig. 5) have comparable mineral characteristics with few variations. The microphotographs of some selected sandy layers (S5, S32, S35, S40, S45, S57) are shown in Fig. 7. Major minerals in the layers include quartz, feldspar,

Table 2 Sample details, dose rate and OSL dates of the three samples of Shey section, Leh Ladakh

Sample	U (ppm)	Th (ppm)	K (%)	Dose rate (Gy/ka)	Paleodose (Gy)	Avg. age (ka)
Top	2.1	6.5	2.1	2.92	99 ± 62	34 ± 21
Middle	2.5	11.2	2.1	3.389	139 ± 48	41 ± 14
Bottom	1.7	6.8	2.3	3.306	172 ± 22	104 ± 8

Moisture content of 10 ± 5% was assumed for all samples and grain size of 90–150 microns

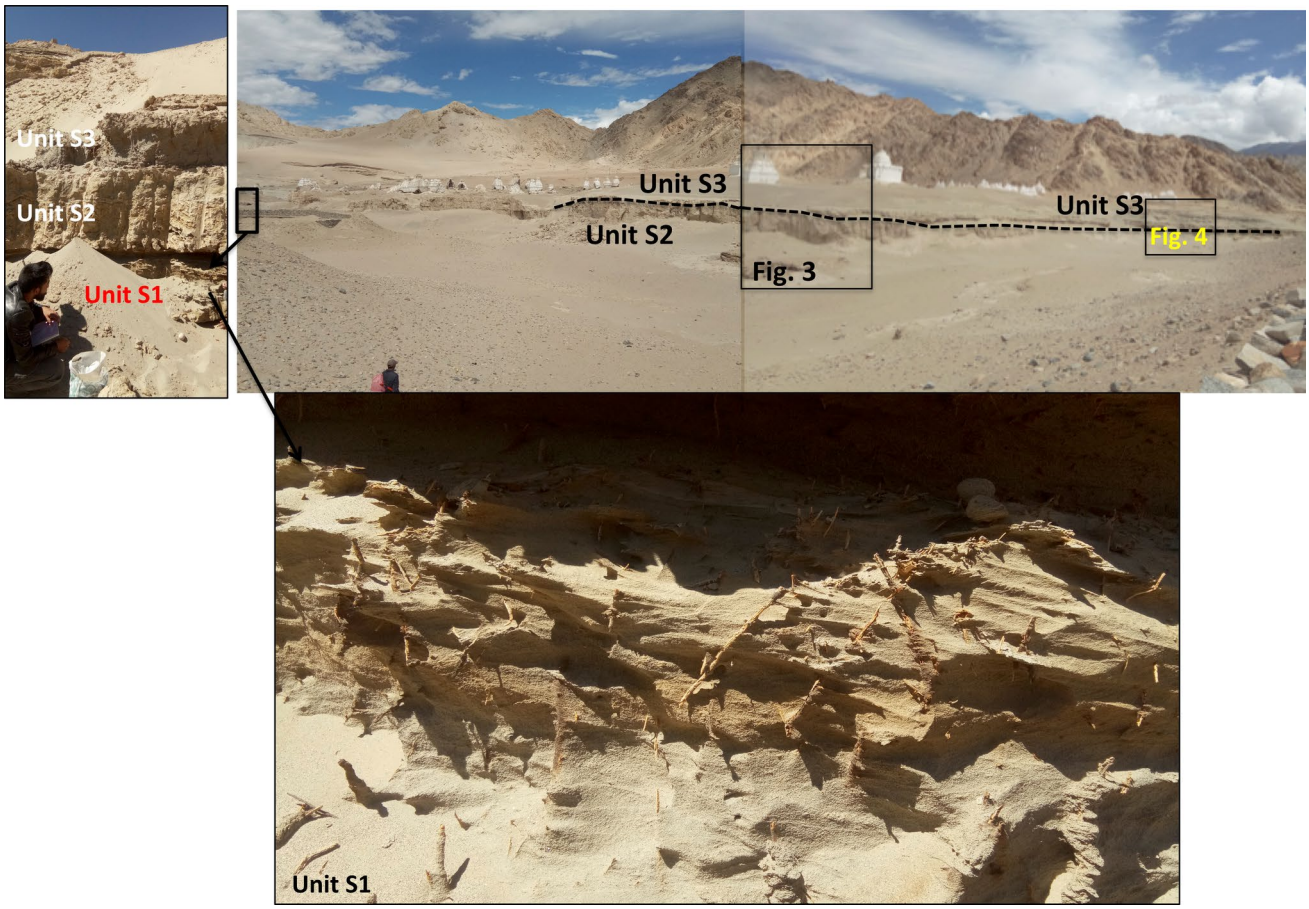

Fig. 2 Panoramic view of the paleolacustrine Shey section showing major units demarcated by erosion surface. Undulating and jointing/faulting structures, slumping of the blocks are seen. The laminated clay bed (S2) is overlain by a sandy S3 unit. A closer view of the three units in the left end of the valley is also provided showing the root traces and sandy nature of the S1 unit

muscovite, biotite, and chert. Some minor amounts of amphibole, chloride, orthoclase, microcline, plagioclase, and pyroxene are present in the sample S35. The layers have a medium- to coarse-grained and well-sorted texture with intergranular space filled with a fine matrix. Oolite structures indicate the amount of carbonate content and channels are lined with a $CaCO_3$ coating. The layers show the presence of root traces and are rich in organic matter (Fig. 7). The long structures may contain some fossils or their traces. Rock fragments embedded within abundant ferruginous fine material are present. Sample S35 and S40 shows abundant circular structures, possibly fossil shells and microfossils. Overall, the sediments have medium to coarse grain, angular to subangular texture, and are randomly striated. A well-sorted arrangement of grains indicates transportation. Therefore, sandy layers have rock fragments, slightly altered grains, abundant Fe/Mn oxides and opaque minerals, and oxidised matter and organic material with no major fossil traces.

Sediment magnetism

Magnetic susceptibility

The magnetic susceptibility of the Shey section shows higher values in all the samples, indicating a good concentration of ferromagnetic and paramagnetic minerals. Susceptibility, expressed as dimensionless χ, varies from 0.1×10^{-3} to a maximum 5.7×10^{-3} with a mean value of $1.8\pm2\times10^{-3}$. The susceptibility of the average mudrocks and that of the Shey sediments are plotted (Fig. 8). The values are significantly different for the clayey and sandy layers of the section. The χ of sandy layers is higher than the clayey layers (average values are plotted). The clayey layers generally show susceptibility range of $\chi=0.1$ to $<2.9\times10^{-3}$. A higher value is also observed in some layers (e.g., $\chi=1.3\times10^{-3}$ in S24) as compared with the average clay S2 unit. On the other hand, sandy layers show higher χ values in the range of 2.9×10^{-3} to 5.7×10^{-3}. Mudrock or mudstones are generally composed

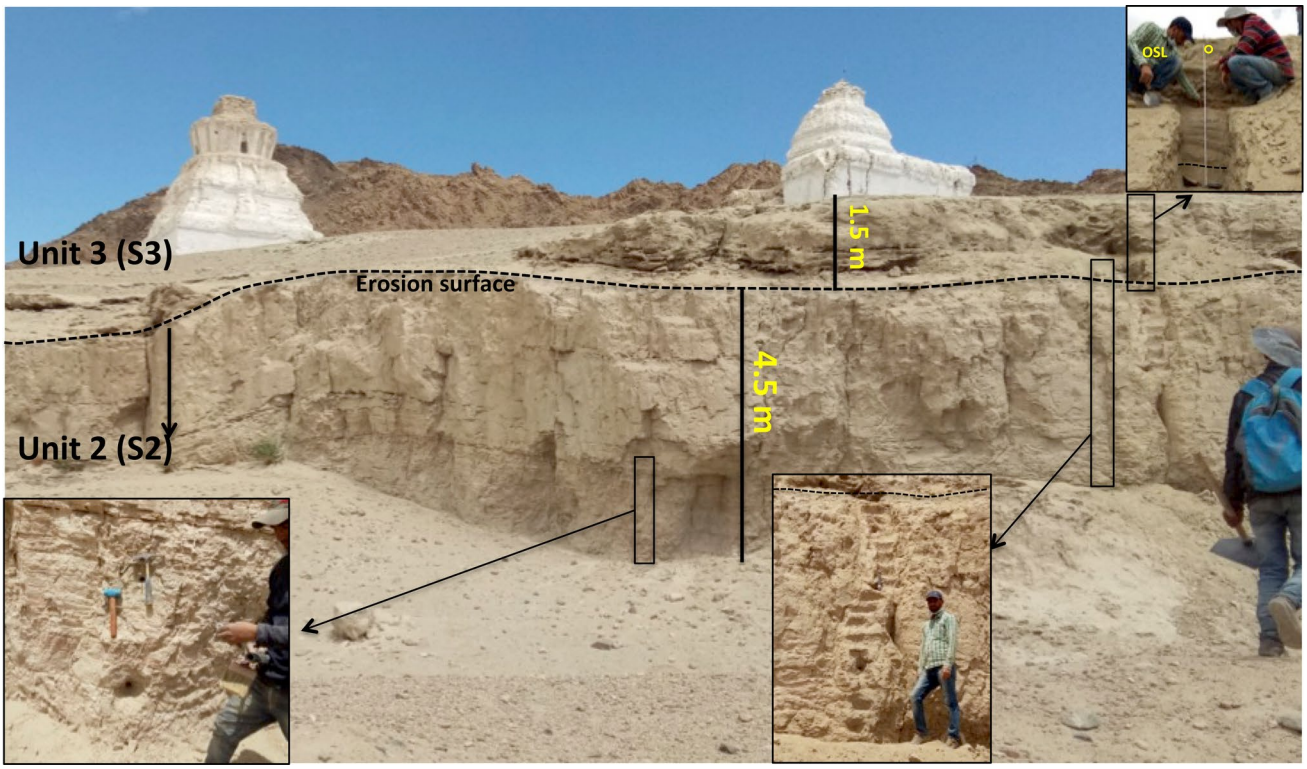

Fig. 3 A detailed view of the S2 unit and the overlying S3 unit in the middle of the Shey section. The layer-to-layer variations of variegated and laminated clay facies can be clearly seen

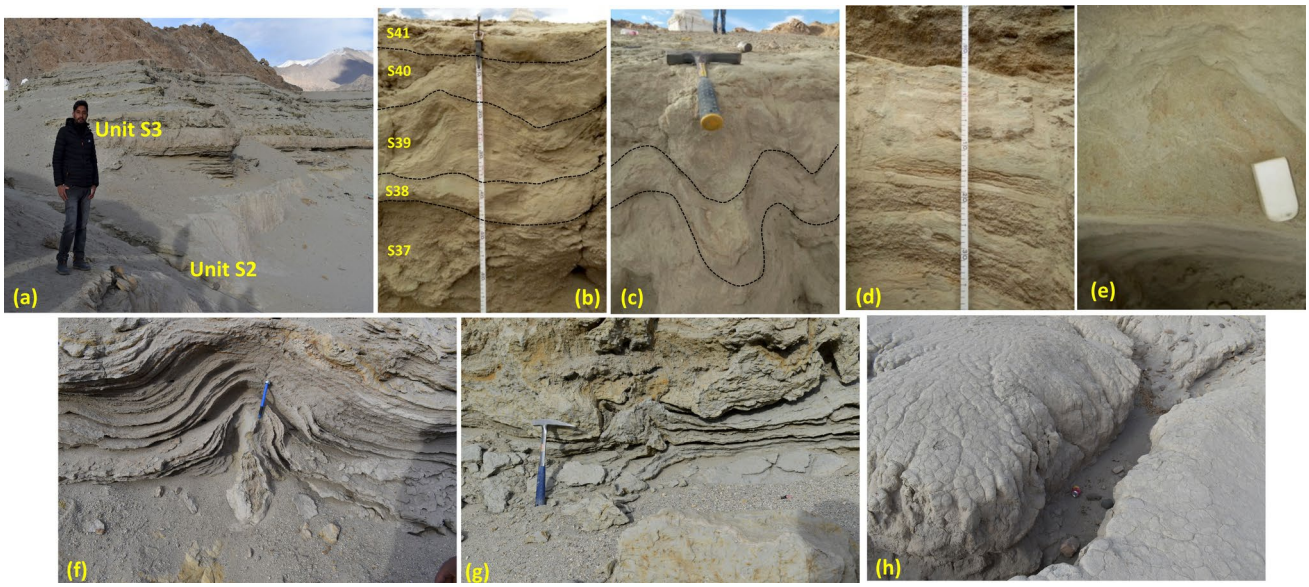

Fig. 4 Field photographs from the top S3 unit showing variation in sediment characteristics **a** general view of the S3 unit showing the deformation and tilting towards East, **b** alternating layers showing soft sediment deformation in different units, **c** convolution structures in the S40/S41, **d** prominent intercalated clay bed (S33), **e** root traces and organic matter in S35, **e**, **f** microstructures in S28-S32 layers, and **h** typical channel/gully erosion in soft sediments

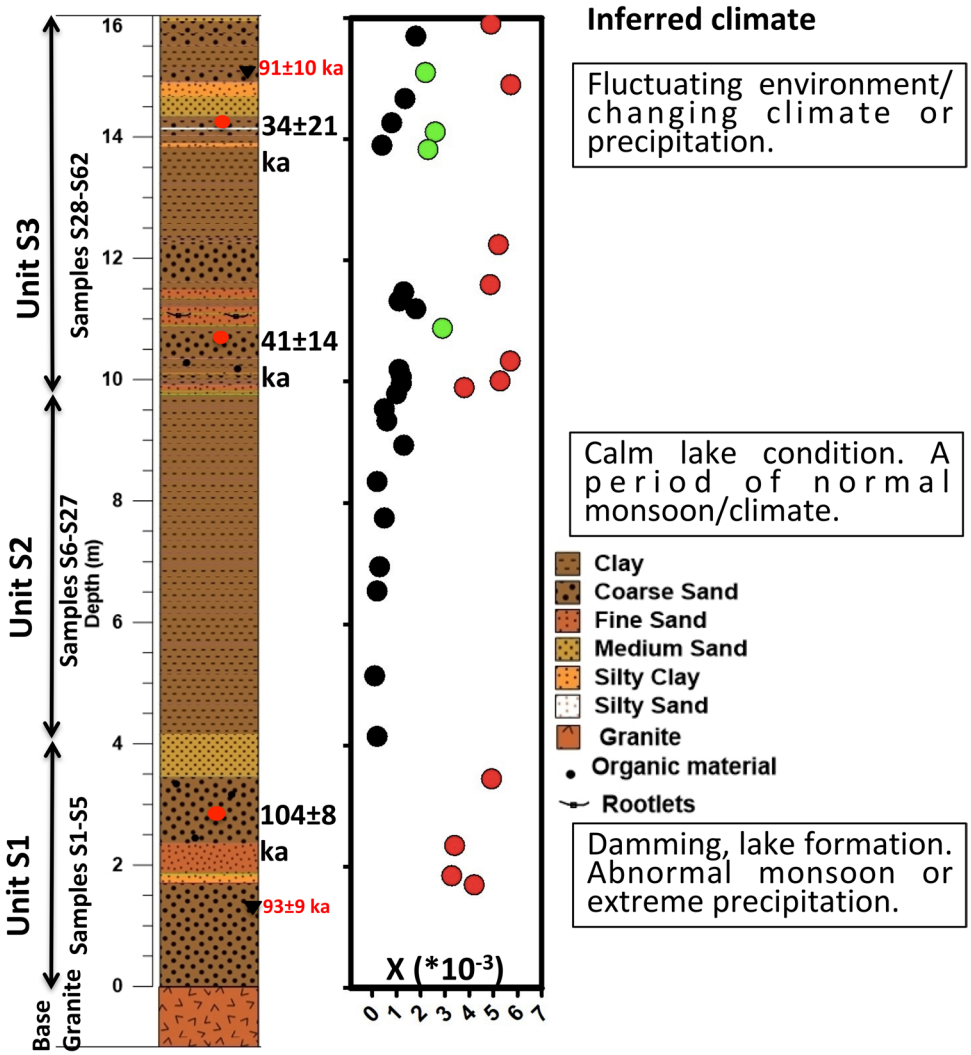

Fig. 5 Figure showing the lithology, sample details, OSL ages from this study (red dots) as well as estimated by Mujtaba et al. (2018) as shown in red text (black triangles), and major environments of deposition. The magnetic susceptibility values are also plotted on the right side

of clay minerals (average 42%), silt-sized quartz (38%), and less than 5% of other minerals like feldspar, calcite, plagioclase, and pyrite (Parés 2015). The average magnetic susceptibility of the mudrocks ranges from 10^{-4} to 10^{-5} (Parés 2015). The χ values are plotted against respective samples in Fig. 5. The susceptibility values of the sediments are also a magnitude higher than the Spituk sediments (range 0.4 to 35×10^{-8} m^3/kg, Sangode et al. 2013).

Hysteresis loops

The shapes of the representative hysteresis loops (Fig. 9) show large variability in width ranging from wider to thinner. In general, all the hysteresis loops are saturated mostly around 3000 Oersted (Oe) and show low coercivity values (less than 200 Oe). A large variation is observed in the magnetic data and parameters of the individual samples, based on which the clayey, sandy, and the layers with mixed grain size show differing and contrasting signatures (Table 3 and Fig. 9a–c).

In clayey samples, the hysteresis loop is wider (open). The samples also attained a very low magnetic saturation (0.6–45 Oe) that too at a higher applied field (7000–8000 Oe). The coercivity and remanence values are also slightly higher as shown for selected (S27, S42, S47, and S54) clayey layers (Fig. 9a). These layers are predominantly composed of fine clay matter.

The sandy and silty layers have almost similar magnetic parameters with minor differences. All the loops are saturated at 3500–4000 Oe but the magnetic bulk density value is higher than the clayey layers (Fig. 9b, c). The selected samples S5, S32, S57, and S62 (Fig. 9c) shows that the hysteresis curves are very thin (closed-loop) with very low coercivity and remanence. The size of the sediments is coarse sand with pebbles. In the layers such as S3, S52, and S55 the loops and other values are intermediate (Fig. 9b). These samples have a grain size between silt to medium sand.

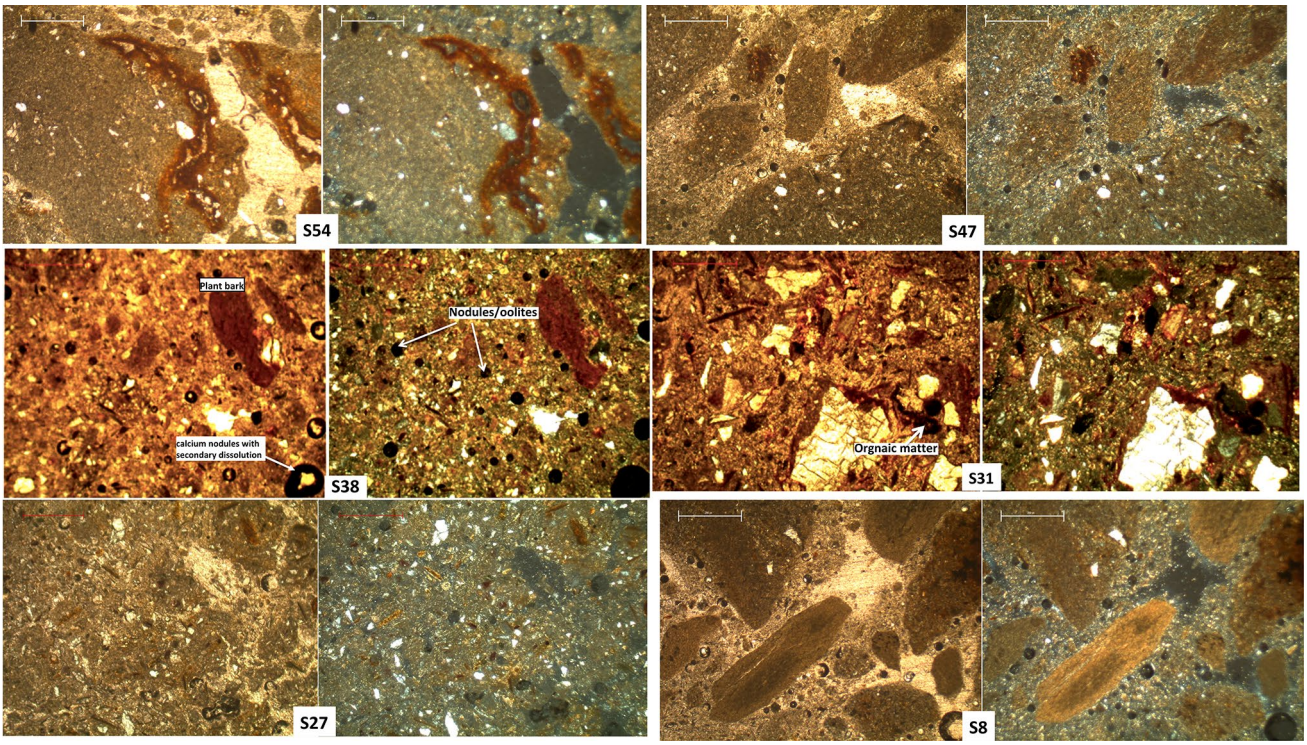

Fig. 6 Photographs of thin sections of representative clayey layers of the section. The left picture of each slide is taken under plane polarised light and the right one in crossed nicols

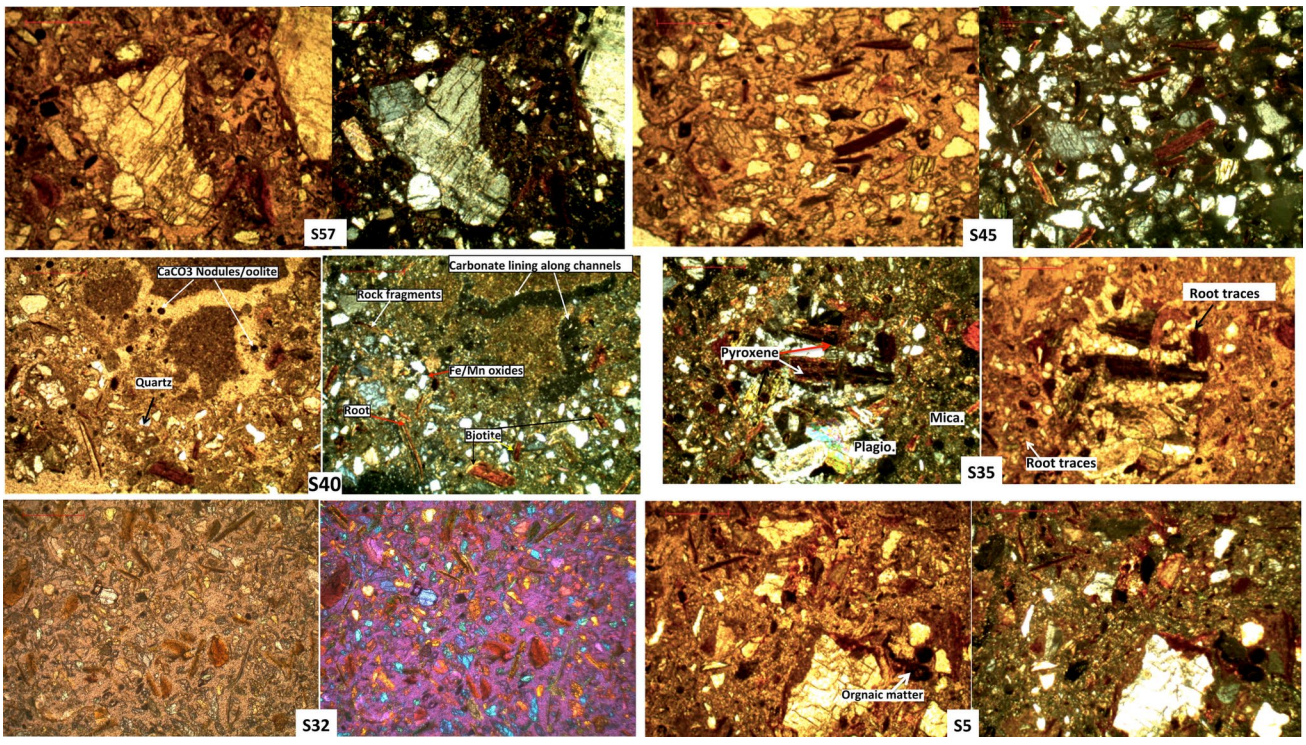

Fig. 7 Photographs of thin sections of representative sandy layers of the section. The left picture in each thin section is under plane polarization and the right ones are taken in crossed nicols

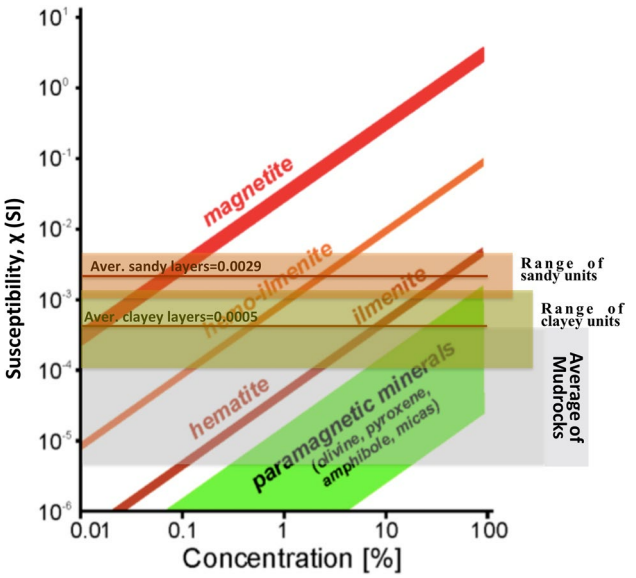

Fig. 8 The relationship between magnetic susceptibility of minerals and their concentration in different rocks (refer to, Hrouda and Kahan 1991; Jackson et al. 1998). The plot estimates the susceptibility contribution by different mineral types or vice versa. For example, in a rock composed of paramagnetic silicate minerals, the contribution of magnetite will be less than 1%

Thermomagnetic curves

The thermomagnetic data of the three types of sediment layers (clay, silt, and sand) also varry greatly and are shown in Table 3. The representative thermomagnetic (K-T) curves of the above-discussed sample types are shown on the right side of Fig. 9. The figures indicate that the heating and cooling curves are very far apart in the clayey layers, closer in the silty samples, and very close in the coarse-grained sandy samples. In all the silty and sandy layers, the cooling curves have susceptibility much lower than the heating curves (the blue curve lying below the red one can be seen in Fig. 9), indicating the stability of magnetic phases. However, the fluctuations in the heating phase of the clayey layers indicate a transformation from stable to unstable phases, like maghemite.

Discussion

Sediment setting

The geomorphic features like granite ridges, alluvial fans, glacial moraines, etc. have an important role in the deposition and preservation of the lacustrine sediments in the area. The topographic setup near the remnant lacustrine sections such as the Spituk, Shey, etc. suggests that the sedimentation in the Leh Valley occurred in separate lake-damming events. The geomorphic map (Fig. 1a, c) shows that at four sites a granite (batholith) ridge from the north and an alluvial fan from the south (Indus formation) almost touch each other (Figs. 1b, 10). The width of the Indus Valley at these locations is very narrow (0.4–1 km) compared to the sites where it shows meandering and braided channels. This indicates that the fan material coalesced with the ridge spurs and created separate lakes at different time periods. The sections are preserved at the shadow zones around these ridge-fan unions (Fig. 10). The largest profile is the Spituk (near Leh airport) and the Army check post site which extends for ~ 6 km. A large colluvial/alluvial fan occurs opposite Phyang village and near the Sabo and Shey sections (opposite Choglamsar). The elevation data shows that the fan near Spituk is about 118 m thick and 291 m near Choglamsar. The southern fan has been incised by the river erosion and created a vertical cliff with a height of less than 10 m in the upstream (Karu side) to more than 32 m in the downstream. Thus, the southern alluvial fans extended to the valley bottom, touched the granite ridges, and created dam conditions in the past. Similar observations can be drawn from a recent study in the area (Jena et al. 2022).

Earlier studies (e.g. Mujtaba et al. 2018) inferred that a single damming event deposited the sediments at several places in the region. From Karu in the southeast to the Phey village, the Indus River has a relief (elevation difference) of 165 m i.e. a gradient of 0.004. Assuming that the river was dammed near Zinchen and created a single lake, the deposition of separate sediments e.g. ~ 60 m thick near Spituk, ~ 16 m near Shey, and other places with differing characteristics and ages is questionable. Therefore, the location and the correlation of their units also indicate that the sections were deposited in the separate damming events in the valley.

Proglacial lakes are created due to the damming of the course of a rivers or melt water flow by four ways during the deglaciarization process (Tweed and Carrivick 2015). The depth, size, and timing of the lakes also depends on various factors (Scherrenberg et al. 2023). The lakes acted as sinks and deposited varied sediment types transported from glaciated catchments (Vergnano et al. 2023). We believe that the combined influence of bedrock, moraine, and debris flow damming created the Shey and other similar proglacial lakes in the Ladakh Himalaya. These factors made these lakes live for millennial time scales as suggested in Tweed and Carrivick (2015).

Environment of deposition

The sedimentation profile indicates that deposition occurred in the three major cycles. After the damming event, the S1 unit was deposited over the Ladakh batholith. The unit, 0–4.15 m thick, grades from medium to coarse sand with

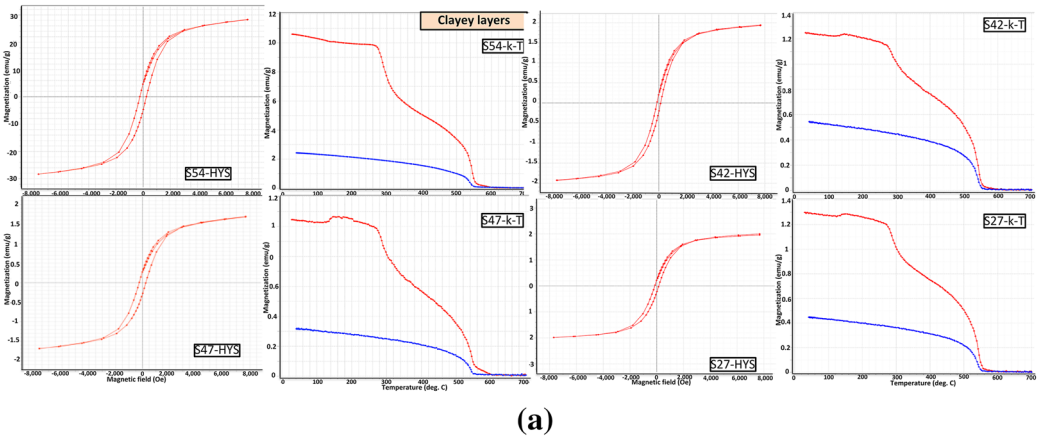

(a)

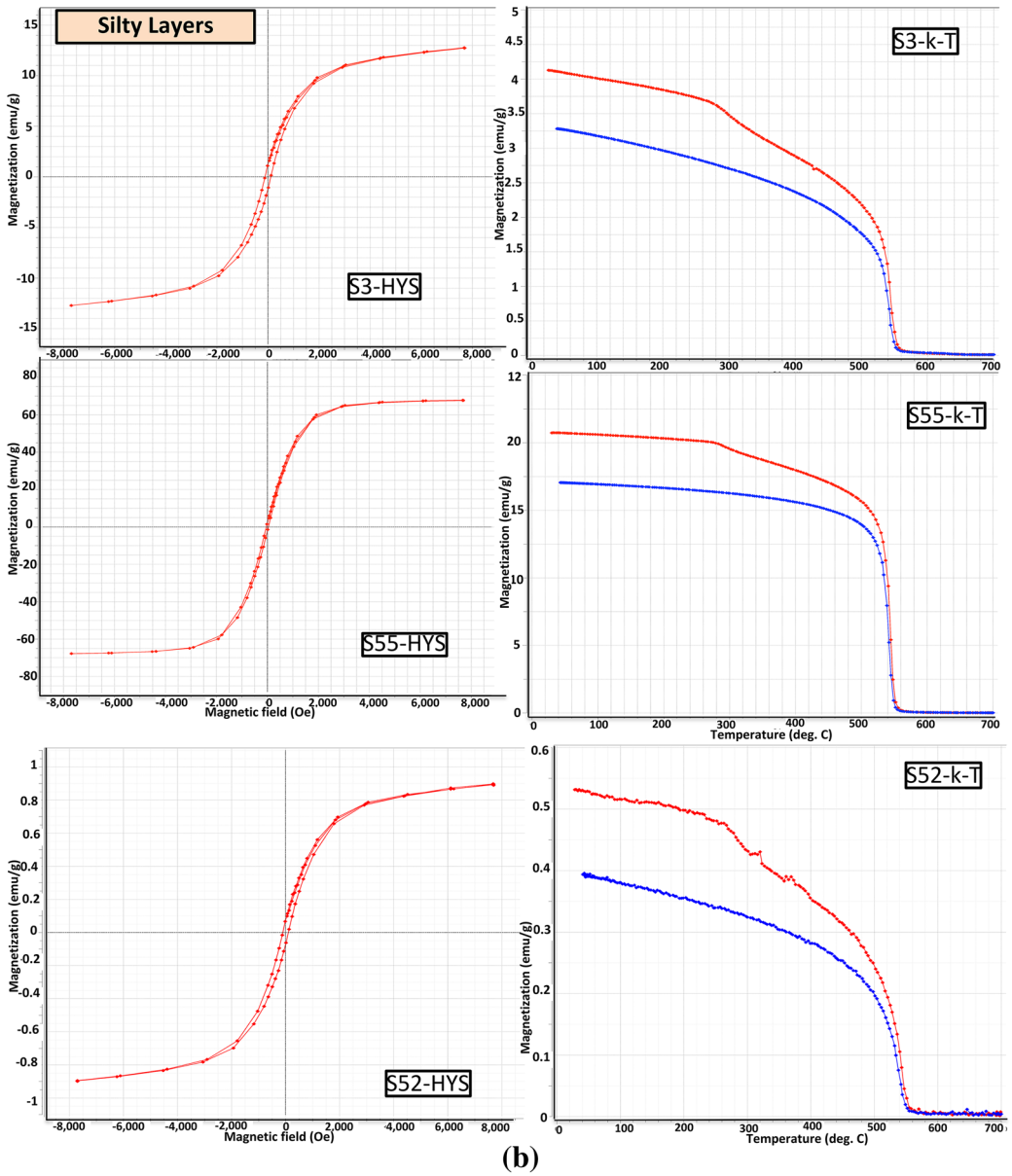

(b)

Fig. 9 **a** Magnetic hysteresis and K-T curves of representative clayey layers of the section. **b** Magnetic hysteresis and K-T curves of representative silty layers of the section. **c** Magnetic hysteresis and K-T curves of representative sandy layers of the section

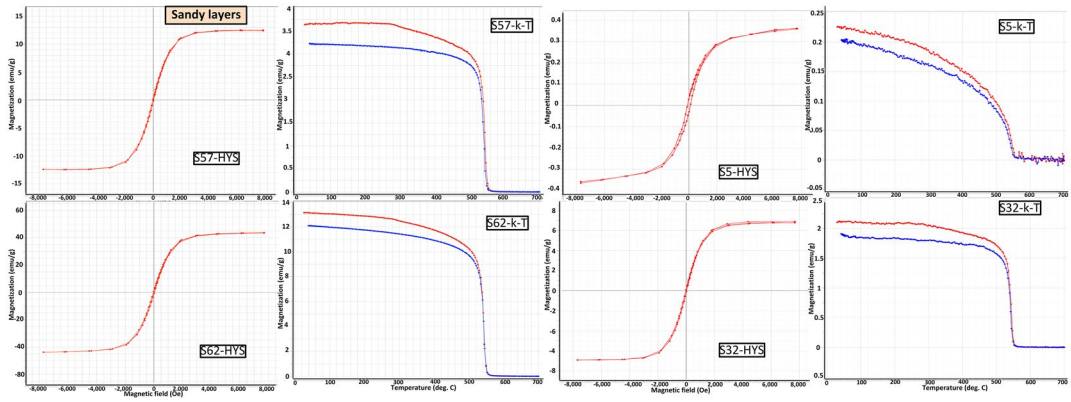

(c)

Fig. 9 (continued)

Table 3 Magnetic properties of the three sediment layers of differing characteristics of the Shey paleolake sediments

	Clayey layers	Silty layers	Sandy layers
Samples	S27, S42, S44, S47, S48, S50, S52, S54, S56, S58, S60	S2, S3, S39, S43. S49, S52, S55	S1, S4, S5, S57, S59, S61, S62
Major composition	Clayey, organic matter rich, laminations, rootlets	Fine to medium sand/silt, no organic matter or pebbles	Coarse sand with pebbles of ~ 2–3 cm diameter
Hysteresis curves	Wider, closes at ~ 3000 Oe. gentle slope after cooling	Medium, closes at ~ 3000 Oe. steep slope after cooling	Narrower, closes at ~ 3000 Oe. steep slope after cooling
Coercivity [Oe]	Generally less than − 200	Generally < − 100	Generally < − 50
Magnetic saturation value	0.6, 0.8, 20, 1.5, 1.5, 2, 30, 35, 45, 40	2, 1, 1.5, 100, 1.5, 80, 0.46, 0.4, 10, 6, 0.3	15, 6, 3, 40
Magnetic saturation attained	Very gently	Gentle to Sharp	More sharply
Magnetic saturation at applied Field [Oe]	7000–8000	3500–4000	3500–4000
Heating/cooling cycles	Very wide or curves far apart	Medium width heating/cooling curves	Very close curves
Susceptibility loss on heating	At 300 T	No loss in both curves	No loss in both curves
Susceptibility becomes zero on heating	At 550 °C	At 550 °C	At 550 °C
Cooling cycle	Starts earlier than 550 °C	Also starts at 550 °C	Also starts at 550 °C

coarser at the base. A band of 65 cm of fine sand to silt (S3 layer) is present in the middle of the unit. In addition, abundant organic material is present in the unit. This indicates fluctuating conditions, increased flow velocity, high-energy conditions, and a high rate of deposition immediately after the damming of the site.

After the stabilization of the depositional environment, the sediments accumulated as the S2 unit (4.15–9.55 m) and the lake reached its maximum size of about 5 km^2. The unit comprises laminated/varved sediments with no major change in color and grain size between the layers (Fig. 3). The clay-sized sediments overall symbolize a single bed representing one major deposition cycle and the presence of thin varves indicate seasonal/annual fluctuations. These characteristics indicate a calm lacustrine environment. The yellowish color indicates the presence of limonite and seasonal variations in oxygen levels under a reducing environment. Compared to its counterpart at the Spituk (Sangode et al. 2013), the middle unit here is coarser and has no dark black layers, indicating that the two sections correspond to separate events.

The topmost S3 unit from 9.55 to 16.5 m (Fig. 5) consists of cyclic and thin alternate sandy and clayey layers indicating sporadic fluvial-lacustrine conditions. The unit also clues high sedimentation rates and rapidly fluctuating environmental/climatic conditions in the catchment. The sandy layers represent warm and/or high precipitation years. The presence of organic matter and root traces (Fig. 5), e.g. in the S35 and other layers, indicates a change

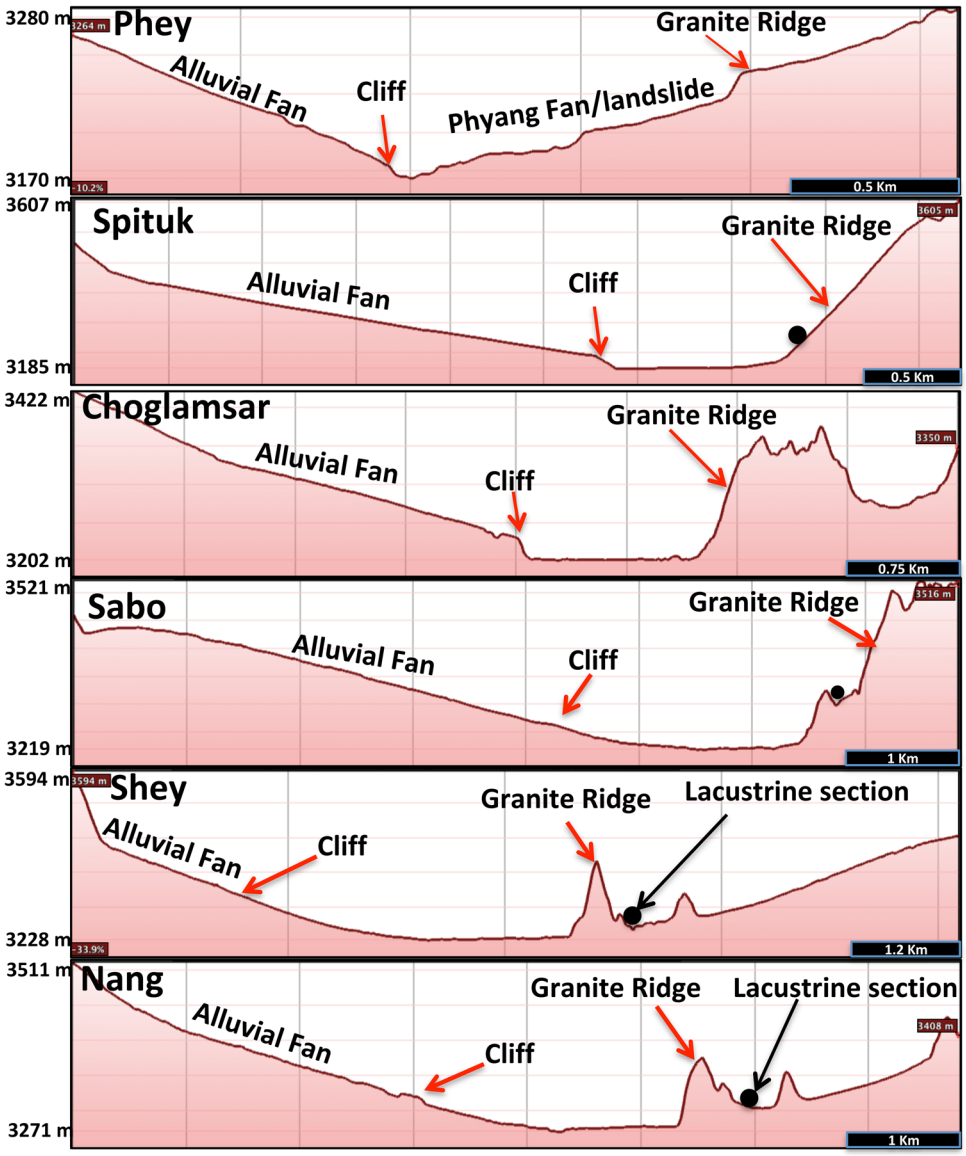

Fig. 10 Topographic profiles along the Leh valley show ridge-fan coalesces where most of the paleolacustrine sections are currently preserved. The profiles were generated using Google Earth Engine

in the environment. Similar features at different depths infer a humid climate or vegetation in the catchment. This high-altitude area remains cold and receives precipitation mainly as snow. Vegetation also remains limited during the cold periods. Therefore, sediment flux in the streams remains less that was deposited as fine clayey matter with little organic activity. The warm or abnormal precipitation phases (e.g. Bookhagen et al. 2005) enhanced the rate of erosion and transported huge material consisting of coarser sand downstream under the stronger runoff conditions (fluvial activity). During these phases temperature remained moderate, which favours vegetation growth (root traces are common) and more sediments. However, the presence of the oolitic fossils-like structures from 12.5 to 13.5 m depth indicates a pure and calm lake setting. The rest of the section shows sporadic fluvial-lacustrine conditions implying that these layers might represent periods when catchment intermittently delivered sediments to the lake environment. Deformation structures, tilting of beds, and the presence of micro folding and faulting, convolute structures, and clay lenses are particularly present in the S3 unit (Fig. 4). These structures are common in similar sediments and are possibly related to the draining of the lake (e.g. Sangode et al. 2011) or seismic activity in the region (e.g. Phartiyal and Sharma 2009; Mujtaba et al. 2018).

Mineralogy and provenance

The presence of biotite, amphibole, quartz, muscovite, k-feldspar, and opaque minerals, which are common in the Shey sediments, cannot be assigned to any particular source rock type. Most of the grains are angular to subangular

indicating less transportation and local provenance. However, according to Lal et al. (2018), the sediments at the Spituk section may have been sourced from the metapelitic rock of the Karakoram Metamorphic Complex, TsoMorari Crystalline Complex, Zildat Ophiolitic Mélange. They observed that the minerals in the lower unit were transported from long-distance metamorphic and magmatic rocks and the middle and upper units from adjoining magmatic geology. The provenance could have shifted from nearby catchments during weaker/normal ISM periods to far-off sources during abnormal or wetter periods (Srivastava et al. 2013).

The lacustrine environments generally deposit highly weathered matter that mainly includes clay and silt-sized particles. The higher χ values in the Shey section than the Spituk sediments indicate the strong ferromagnetic nature of the sediments, low transportation and a strong ferromagnetic nature due to magnetite (Sangode et al. 2013). Large variations in these characteristics of the two sections, therefore, indicate different and nearby or local sources of the Shey sediments. The clayey units (Fig. 6) with rock fragments, angular grains, fresh minerals, and low alteration of grain boundaries (low physical weathering or alteration) also indicate a local glacial provenance.

Furthermore, the common minerals present in the Shey sediments are quartz, feldspar, muscovite, biotite, pyroxene, and a minor amount amphiboles, chert, chlorite, and microcline. The mineral assemblage is embedded in a fine clay matrix. The clayey layers also show large amounts of carbonate matter, which is biogenic in the form of oolites, fossil shells, etc. The catchment includes the fossiliferous limestone from which these carbonates have likely been transported. The sandy layers are rich in chert and iron oxides. Thus, the bulk susceptibility of the Shey sediments depends on the susceptibility of the constituent minerals and their proportion. The susceptibility of the average mudrocks, major magnetic minerals, and that of the Shey sediments are plotted (Fig. 8). The higher χ of sandy layers than the clayey layers indicates a higher concentration of magnetic minerals such as magnetite and maghemite in these layers. Similarly, the major magnetic minerals in clayey layers are mainly paramagnetic silicate minerals including quartz, feldspar, pyroxene, amphiboles, and micas. According to Sangode et al. (2013), the yellowish-grey sandy matter in the Spituk section is ferromagnetic, which indicates the ferrimagnetic nature of the granodioritic batholithic source. While the antiferromagnetic and mixed ferromagnetic sands are dark grey and indicate the Indus molasses source. The susceptibility in these dark layers is mainly due to organic matter and an abundance of paramagnetic minerals. Figure 10 indicates that the clayey units of the Shey section are rich in paramagnetic silicate minerals, which are also observed in the thin sections. Thus, the non-resembling provenance indicators of the two sections also suggest that the Shey Lake formation was a separate event.

The clayey and sandy layers also show differing characteristics. The clayey layers (whole S2 unit and thin intercalated clayey layers in S1 and S3 units) are low in organic matter and show a good amount of carbonates in the form of oolites, fossil shells, and $CaCO_3$ coated channels. The layers have low susceptibility ($\chi = 0.1$ to $< 2.9 \times 10^{-3}$). High carbonate matter, which is normally diamagnetic, and less detrital magnetic and silicate input are mainly responsible for low susceptibility per unit volume or mass in the clayey beds (Li et al. 2006). A higher value ($\chi = 1.3 \times 10^{-3}$) in the reddish S24 of the S2 unit is because of iron oxides. This possibly indicates chlorite weathering, which releases Fe and forms strong magnetic oxides such as maghemite and even hematite (e.g. Ye et al. 2020). Chlorite is susceptible to weathering and is common in the Spituk sediments (Lal et al. 2018). The thin sections of the layers also show large altered grains suggesting the extent of weathering. These clay layers represent cold, low precipitation phases and calm lake settings. The cooler climate hinders the upland vegetation and aquatic vegetation to flourish. These cooler events generate fine sediments brought by glacial melt-water with low sediment supply. This sedimentation phase continued with no major change or increase in the precipitation. In contrast, the silt/sandy layers possess organic matter, root traces, and iron oxides, and have a yellowish color due to chlorites. A high amount of angular clastic matter (pebbles, etc.) suggests more erosion and rapid sedimentation and flow conditions. The grains are well sorted due to large transportation. More vegetation matter indicates increased temperature. High χ in silt/sandy layers indicates an increase in magnetic concentration, which reflects a shift to a high-flow environment and high precipitation with mainly snow (Vlag et al. 1997). The magnetic concentrate maxima also corresponds to warm periods during which the area generally had more vegetation cover hence high organic content and yielding high clastic erosion (Thouveny et al. 1994; Jelinowska et al. 1997; Lanci et al. 1999).

Similarly, the magnetic data (Table 3 and Fig. 9) provides information about the grain size and mineral content in the different layers. In general, all the hysteresis loops are saturated mostly around 3000 Oersted (Oe) and show low coercivity values (less than 200 Oe). This indicates the predominance of ferromagnetic components, i.e., magnetite in all the samples of the section (e.g. Jackson et al. 1989). Magnetite is generally an opaque black and hematite reddish brown mineral in thin sections.

In the clayey layers, the wider (open) hysteresis loop, very low magnetic saturation at higher applied field, high remanence, medium to high coercivity suggest predominance of paramagnetic or antiferromagnetic or

magnetically hard minerals like haematite that occur as dominant magnetic state in Single Domain (SD) fine grains (Evans and Heller 2003; Basavaiah and Khadkikar 2004; Kapawar and Venkateshwarlu 2020). These values suggest a typical nature of good amount of antiferromagnetic hematite with ferromagnetic magnetite. While, in the layers of silt to coarse sand, very thin (closed) hysteresis curves, very low coercivity, and remanence values, saturation at 3500–4000 Oe and higher magnetic bulk density indicates the dominance of soft magnetic or ferrimagnetic minerals i.e., magnetite (Basavaiah and Khadkikar 2004; Mohamad and Paleologos 2018; Kapawar and Venkateshwarlu 2020). This also indicates a medium-coarse magnetic grain size with a magnetic domain state dominated by Multi-Domain (MD) grains. However a high amount of finer silt in some sandy layers in the section (e.g. S3, S52, and S55) produces intermediate loops and other magnetic values that indicate paramagnetic or antiferromagnetic or magnetically hard minerals like haematite and Multi-Domain (MD) grains.

The K-T curves of the clayey layers possess dual magnetic components and the heating cycles are thermally unstable than cooling cycles, suggesting their irreversible nature. More than one Tc in some samples indicates more than one thermomagnetic element. Magnetite has a Tc of 580 °C. Susceptibility in these samples becomes zero at higher Tc (above ~ 550 °C). However, Tc less than magnetite (~ 580 °C) indicates the presence of a minor Ti-poor titanomagnetite due to the substitution of Fe by Al or Ti in magnetite. These samples show a considerable susceptibility loss in the heating cycle near ~ 300 °C indicating the presence of pyrrhotite (Kapawar and Venkateshwarlu 2020). This drop in susceptibility in heating cycles also indicates the transformation of metastable maghemite to hematite (Maity et al. 2022). The majority of the samples contain primary unstable magnetic phases like maghemite, ilmenite, goethite, and pyrrhotite along with low coercive magnetite, which has a minor contribution in the total susceptibility in the samples (Verosub and Roberts 1995; Mohamad and Paleologos 2018). Ilmenite, maghemite, and goethite are generally the products of weathering and form due to pedogenic processes, which convert paramagnetic minerals to ferromagnetic (e.g. Mohamad and Paleologos 2018). The presence of magnetic minerals in the fine-grained layers indicates their formation when the sediments rich in iron are subjected to alteration in a low-oxygen environment. The ferromagnetic material, which is present in the lake condition for a longer time, also converts to a particular magnetic mineral. Few samples demonstrate an enhanced susceptibility around 100–150 °C indicating the thermal transformation of clay minerals during the heating cycle. In addition, the cooling cycle of the samples starts earlier at ~ 530 °C and this low Tc component likely corresponds to low Ti-titanomagnetite in the group that alters to higher Tc component magnetite.

In the sandy layers, the heating and cooling cycles both start at 550 °C and also show no major sign of susceptibility fluctuations or loss during heating and cooling processes (Fig. 9c). This is the characteristic property of highly stable magnetite. The behavior of cooling curves also does not indicate unstable phases like maghemite or low Ti-titanomagnetite, but the pure magnetite depicts its complete transformation (reversible behavior) after heating (Kapawar and Venkateshwarlu 2020). All this indicates that magnetite is the leading magnetic carrier in these layers, which is also revealed by its Tc ~ 550 °C (Fig. 9).

In the fine-grained silty layers of the section, the magnetic data suggests the presence of at least two magnetic carriers (Fig. 9b). For example, the S3 sample shows a somewhat wider hysteresis loop, minor susceptibility loss at 300 °C on heating, and highly fluctuating K-T curves than the other four layers of the S1. This suggests a mixed nature and possession of both stable magnetite with a considerable amount of unstable minerals such as paramagnetic and antiferromagnetic maghemite, ilmenite, and pyrrhotite in the layers with silt to fine sand grain size.

Age and climate model

The three OSL ages from the Shey section (Fig. 5 and Table 2) range from 104 ± 8 ka (~ 3 m) to 34 ± 21 ka (~ 14 m). The middle S2 unit was deposited at a sedimentation rate of nearly 1 cm per 78.7 years, while the rate of deposition of the upper unit was faster at about 1 cm per 19.5 years. Sharma and Phartiyal (2018) suggest the deposition of about 40 m lake sediments in around 70 ka at the Spituk site. The OSL ages i.e. 93 ± 9 ka to 91 ± 10 ka calculated from the same Shey section (Mujtaba et al. 2018) did not mention the exact depth of the samples however, the results indicate that nearly 16 m of these sediments were deposited in just 3 ka. This faster rate of deposition in the lacustrine environment does not corroborate with our and other studies. Thus we suggest that the Shey Lake was created before 104 ka and the sedimentation continued even after 34 ka.

The Quaternary period between ~ 140–130 ka or MIS 6 has noticed major glaciation all over the world and its end is called the Penultimate Glacial Maxima (e.g. Florence et al. 2016). The period after 130 ka (age 130–70 ka or MIS 5) was an interglacial warm period with three major warmer events (i.e. interstadial 5e, 5c, 5a) when the temperature rose rapidly (Fig. 11). This period showed increased insolation of ~ 500 W/m^2, higher ocean surface temperature, and corresponds with the troughs in oxygen-18 (very low $\delta^{18}O$ values). The Ladakh region also observed similar glacial and warmer events. Some of the important glacial stages of this period e.g. Leh Stage (200–130 ka), Kar Stage (105–85 ka), Pangong-2 glacial

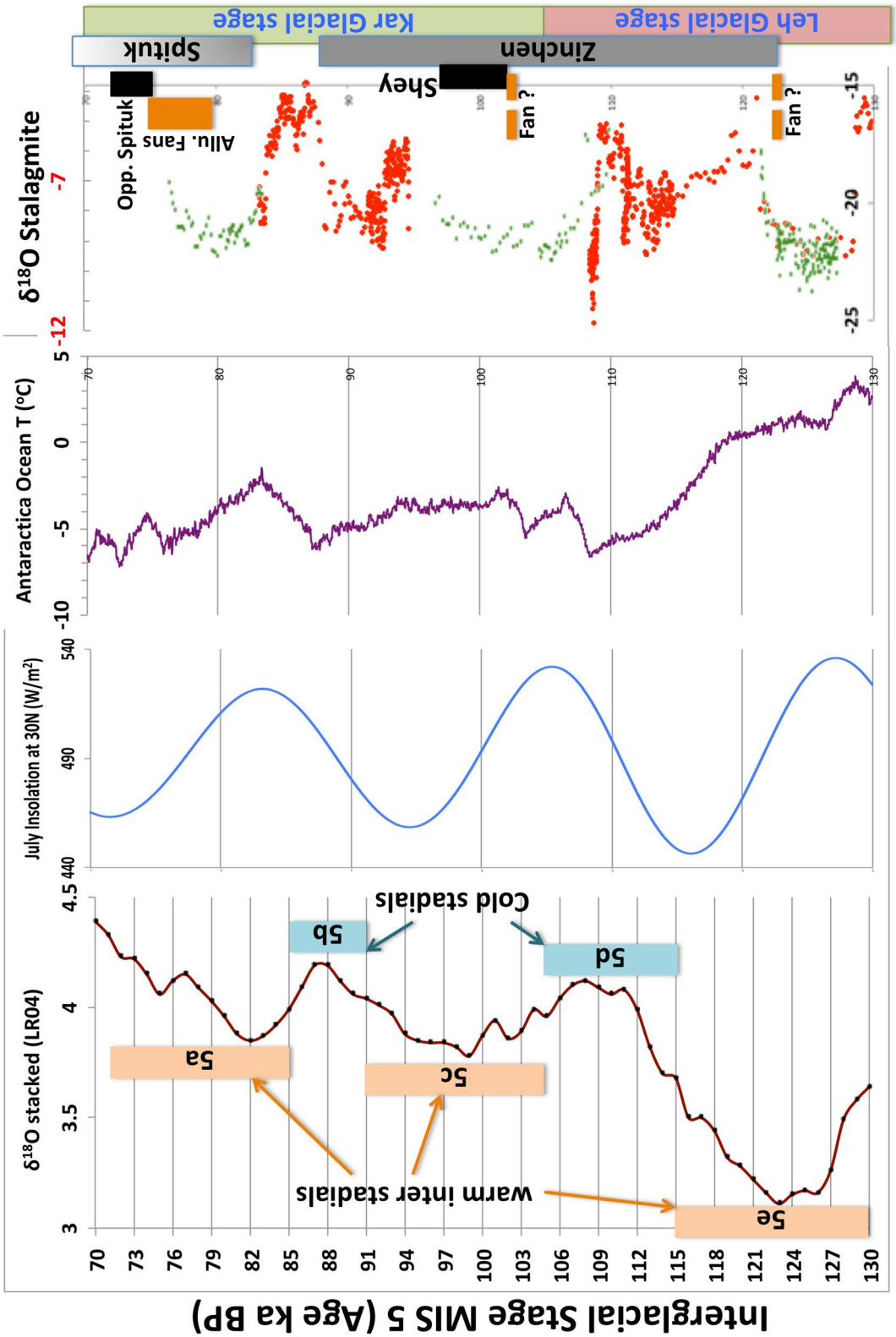

Fig. 11 Plot of data for Marine Isotope Stage (MIS 5) showing similarity of $\delta^{18}O$ record (LR04 stake; Lisiecki and Raymo 2005), Summer insolation at 30° N (Laskar et al. 2004), Antarctica Ocean Surface Temperature (Parrenin et al. 2013), and $\delta^{18}O$ record of stalagmites from Bitto Cave Himachal Pradesh (red dots; Kathayat et al. 2016) and Tianmen cave Tibet (green dots; Cai et al. 2010). Also shown are a few past lake sediments from Leh valley and glacial stages of this period (Owen et al. 2006). The data sets were archived from: https://www.ncei.noaa.gov, https://dbpedia.org, and https://www.pangaea.de

stage (~ 85 ka), and Ladakh Stage-4 (~ 81 ka) have been dated by various workers (Fort et al. 1989; Brown et al. 2002; Owen et al. 2006; Dortch et al. 2011). Although two minor cooler events also occurred, overall a rise in temperature initiated fast glacial melting in the Ladakh region and transported huge material downslope.

From our results and other studies (Mujtaba et al. 2018; Sharma and Phartiyal 2018), it is possible that during the warm MIS-5 stage, Leh also observed very frequent lake deposition events, which are preserved in the Valley and outside (Table 1). During this warm interglacial period, the Indus River dammed at many places by the weathered material attributed to processes such as rainfall-induced debris flows (Phartiyal et al. 2005; Sant et al. 2011a, b; Fort et al. 1989; Sharma and Phartiyal 2018), glacial moraine (Sangode et al. 2011), alluvial fans (Blöthe et al. 2014), and landslides (Mujtaba et al. 2018). Leh Valley has observed various major glaciation periods in the past with some covering the whole valley area (e.g. Sharma and Chand 2016; Shukla et al. 2020). Glaciers have advanced during these periods due to enhanced moisture contributed by Westerlies and ISM (Jena et al. 2022). Overall the response of the glaciers in the Himalayan region is attributed more to the ISM changes than the MLW fluctuation (Arora et al. 2023). One such widely accepted blockade by a huge alluvial fan created a lake between the Phyang and Spituk and deposited the material with conglomerates at its base. The date of the fan (ref. Table 1) correlates with a warm interstadial (5a) event (e.g. Table 2 and Fig. 11). Similarly, another section correlates well with a warmer event (e.g. 5c). The Shey blockade is another example where debris flow or colluvial/alluvial material dammed the river near Stakma stream. The date of the section corresponds with the peak 5c warm period (Fig. 11). The sedimentation in the lake was active around 100 ka and its three units indicate three different paleo-environments caused due to minor fluctuations. The MIS-5 is characterised by short-lived millennial-scale climatic fluctuations of enhanced moisture and dry events. These fluctuations caused the expansion and diminishing of valley glaciers and temporal changes in the meltwater discharge. This paleohydrological fluctuation caused the variation in the lake sedimentation in the relict lake. The warm events also correlate well with the rising global temperature, isotope data, and cave stalagmite isotope data from nearby areas. Generall, the lower delta ^{18}O values or increased heavier isotopes corresponding to the rising temperature. This indicates that the Ladakh region witnessed an abnormal monsoon period or extreme precipitation event as well as rapid melting of glaciers. The study of such processes is also important to model the vulnerability of the region to catastrophic hydrological hazards (e.g. Sharma et al. 2021). Similar events of low magnitude have caused large-scale destruction of the environment in recent years in the region (Ziegler et al. 2016).

Conclusion

The sediments preserved at the Shey village of semi-arid Ladakh Himalaya indicates that the colluvial/alluvial fan material from the southern hills coalesced with a granite ridge and blocked the Indus during the MIS-5 warming phase of the LGM. This temporary damming created a lacustrine environment over ~ 5 km^2 area in which sediments were deposited in three units. The lower coarser unit represents fluvial-lacustrine conditions, the middle clayey bed represents the lacustrine environment, and the uppermost unit, comprising fluctuating fluvial-lacustrine layers, indicates an abruptly oscillating climate. Hysteresis loops and K–T curves indicate that the dominant magnetic phase present in sandy layers with pebbles is magnetite, which occurs as the MD phase and has higher susceptibility but low coercivity and remanence. In the clayey layers, at least two magnetic carriers i.e. stable magnetite with a considerable amount of unstable minerals such as paramagnetic and antiferromagnetic maghemite, ilmenite, and pyrrhotite are present. The Shey section was deposited between ~ ca 100 to 34 ka during the MIS 5c interstadial warm event that has lasted for about 14,000 years and corresponds to the Upper and Late Pleistocene age. The results presented in the study undermine the premise of a single daming event throughout the valley and suggests that a separate lake deposited the sediments for more than 70 thousand years. In contrast to the previous studies the results also shed light on the lake formation due to the combined effects of bedrock, moraine, and debris flow damming. The sediments were transported from a nearby provenance. The results are helpful to reconstruct the paleoenvironment and paleoclimate in the complex Himalayan topography.

Acknowledgements The author (FD) is highly thankful to the University Grants Commission, Government of India (UGC) for providing the UGC-BSR Start-Up grant. The University of Kashmir is acknowledged for all the support provided during the project work. The Directors of CSIR-NGRI, Hyderabad, and BSIP, Lucknow are thanked for the laboratory permission. Akhtar Rasool Mir, University of Kashmiris helped in the thin section interpretation. We are highly thankful to the two anonymous reviewers for their detailed review of the manuscript that improved the quality of the work.

Author contributions Farooq Dar has conceptualized, prepared figures, and wrote the original manuscript. Mamilla Venkateshwarlu performed the magnetic analysis, interpreted the data, and edited the manuscript. Imran Khan helped with fieldwork, sample collection, and data generation. Malik Zubair Ahmad helped with fieldwork and interpretation of the results.

Funding The paper is based on the work carried out under the UGC-BSR Grant No. F. 30-357/2017. "OSL Dating, Carbon Isotope and

Magnetic Susceptibility studies of Lacustrine Sediments of Leh, Ladakh India: Implication on Past Climate Changes in Himalayan region".

Data availability The data generated in the manuscript could be available from the corresponding author on proper request.

Declarations

Conflict of interest The authors declare they have no conflict of interest.

References

Ahn H, Lim J, Kim SW (2021) Magnetic properties of a Holocene sediment core from the Yeongsan Estuary, Southwest Korea: implications for diagenetic effects and availability as paleoenvironmental proxies. Front Earth Sci 9:593332

Aitken MJ (1998) An introduction to optical dating. Oxford University Press, London, p 267

Ali N, Biswas RH, Shukla AD, Juyal N (2013) Chronology and climatic implications of Late Quaternary glaciations in the Goriganga valley, central Himalaya. India Quat Sci Rev 73:59–76

Arora P, Ali SN, Sharma A (2023) Role of different moisture sources in driving the western Himalayan past-glacier advances. J Atmos Sci Res 6(3):1–19

Bhattacharyya A, Sandeep K, Misra S, Shankar R, Warrier AK, Weijian Z, Xuefeng L (2015) Vegetational and climatic variations during the past 3100 years in southern India: evidence from pollen, magnetic susceptibility and particle size data. Environ Earth Sci 74:3559–3572

Bhutiyani MR, Kale VS, Pawar NJ (2010) Climate change and the precipitation variations in the northwestern Himalaya: 1866–2006. Int J Climatol 30:535–548

Blöthe JH, Munack H, Korup O, Fülling A, Garzanti E, Resentini A, Kubik PW (2014) Late Quaternary valley infill and dissection in the Indus River, western Tibetan Plateau margin. Quat Sci Reviews 94:102–119

Bookhagen B, Rasmus C, Thiede M, Strecker R (2005) Late Quaternary intensified monsoon phases control landscape evolution in the northwest Himalaya. Geol 33(2):149–152

Brown ET, Bendick R, Bourles DL, Gaur V, Molnar P, Raisbeck GM, Yiou F (2002) Slip rates of the Karakorum fault, Ladakh, India, determined using cosmic ray exposure dating of debris flows and moraines. J Geophys Res Solid Earth 107(B9):ESE–7

Cai Y, Cheng H, An Z, Edwards RL, Wang X, Tan L, Wang J (2010) Large variations of oxygen isotopes in precipitation over south-central Tibet during Marine Isotope Stage 5. Geol 38(3):243–246

Chaudhary S (2015) Optically stimulated Luminescence (OSL) dating of sediments from Himalaya. J Indian Institute Sci 95:2

Clift PD (2002) A brief history of the Indus River. Geol Soc Lond 195(1):237–258

Clift P, Shimizu N, Layne G, Gaedicke C, Schlter HU, Clark M, Amjad S (2000) Fifty-five million years of Tibetan evolution recorded in the Indus Fan. Eos Trans Am Geop Union 81:277–281

Critelli S, Lepera E, Galluzzo F, Milli S, Moscatelli M, Perrotta S, Santantonio M (2007) Interpreting siliciclastic-carbonate detritals modes in foreland basin systems: an example from Upper Miocene arenites of the central Apennines, Italy. In: Arribas J, Critelli S, Johnsson MJ (Eds.) Sedimentary provenance and petrogenesis: perspectives from petrography and geochemistry. Geol. Soci. America 420:107–133

Dekkers MJ (1997) Environmental magnetism: an introduction. Geol Mijnbouw 76(1–2):163–182

Dortch JM, Owen LA, Haneberg WC et al (2009) Nature and timing of large landslides in the Himalaya and Transhimalaya of northern India. Quat Sci Rev 28:1037–1054

Dortch JM, Dietsch C, Owen LA, Caffee MW, Ruppert K (2011) Episodic fluvial incision of rivers and rock uplift in the Himalaya and Transhimalaya. J Geol Soc London 168:783–804

Evans ME, Heller F (2003) Environmental magnetism: principles and applications of enviromagnetics. Academic Press (**ISBN:978-0-12-243851-6**)

Florence C, Claudia W, Jens-Ove N, Jenny B, Simona M (2016) Constraint on the penultimate glacial maximum Northern Hemisphere ice topography (≈ 140 kyrs BP). Quat Sci Rev 137:97–112

Fort M, Burbank DW, Freytet P (1989) Lacustrine sedimentation in a semi-arid alpine setting: an example from Ladakh, northwestern Himalaya. Quat Res 31:332–352

Galbraith RF, Roberts RG, Laslett GM, Yoshida H, Olley JM (1999) Optical dating of single and multiple grains of quartz from Jinmium rock shelter, northern Australia: Part I. Experimental design and statistical models. Archaeometry 41:339–364

Garzanti E, Van-Haver T (1988) The Indus clastics: forearc basin sedimentation in the Ladakh Himalaya (India). Sediment Geol 59:237–249

Heri AR, Aitchison JC, King JA, Villa IM (2015) Geochronology and isotope geochemistry of Eocene dykes intruding the Ladakh Batholith. Lithos 212–215:111–121

Hrouda F, Kahan Š (1991) The magnetic fabric relationship between sedimentary and basement nappes in the High Tatra Mountains. N Slovakia J Struct Geol 13:431–442

Huang H, Gao Y, Jones MM, Tao H, Carroll AR, Ibarra DE, Wang C (2020) Astronomical forcing of Middle Permian terrestrial climate recorded in a large paleolake in northwestern China. Palaeogeogr Palaeoclimatol Palaeoecol 550:109735

Jackson M, Sprowl D, Ellwood B (1989) Anisotropies of partial anhysteretic remanence and susceptibility in compacted black shales: grain size and composition-dependent magnetic fabric. Geophys Res Lett 16:1063–1066

Jaiswal MK, Srivastava P, Tripathi JK, Islam R (2008) Feasibility of the SAR technique on quartz sand of terraces of Nw Himalaya: a case study from Devprayag. Geochronometria 31:45–52

Jelinowska A, Tucholka P, Wieckowski K (1997) Magnetic properties of sediments in a Polish lake: evidence of a relation between the rock-magnetic record and environmental changes in Late Pleistocene and Holocene sediments. Geophys J Int 129:727–736

Jena PS, Bhushan R, Raj H, Dabhi AJ, Sharma S, Shukla AD, Juyal N (2022) Relict proglacial lake of Spituk (Leh), northwest (NW) Himalaya: a repository of hydrological changes during Marine Isotopic Stage (MIS)-2. Palaeogeogr Palaeoclimatol Palaeoecol. 602:111164

Johnsson MJ (1993) The system controlling the composition of clastic sediments. In: Johnsson, Basu MJA (Eds.) Processes controlling the composition of clastic sediments. Geol. Soc. America 284:1–19

Juyal N (2014) Ladakh: the high-altitude Indian cold desert. Landscapes and landforms of India 115–124

Kapawar M, Venkateshwarlu M (2020) Paleomagnetism and rock magnetism of early Cretaceous Rajmahal basalts, NE India: implications for paleogeography of the Indian subcontinent and migration of the Kerguelen hotspot. J Asian Earth Sci 201:104517

Kathayat G, Cheng H, Sinha A et al (2016) Indian monsoon variability on millennial-orbital timescales. Sci Rep. https://doi.org/10.1038/srep24374

Kolstrup E (2007) OSL dating in palaeoenvironmental reconstructions. A discussion from a user's perspective. Estonian J Earth Sci 56(3):157

Kotlia BS, Shukla UK, Bhalla MS, Mathur PD, Pant CC (1997) Quaternary fluvio-lacustrine deposits of the Lamayuru Basin, Ladakh Himalaya: preliminary multidisciplinary investigations. Geol Magazine 134:807–812

Kumar A, Srivastava P (2017) The role of climate and tectonics in aggradation and incision of the Indus River in the Ladakh Himalaya during the late Quaternary. Quat Res 87(3):363–385

Kumar A, Srivastava P, Sen K, Morell K, Hazarika D (2020) Evidence for late Quaternary brittle deformation and back thrusting within the Indus Suture Zone, Ladakh Himalaya. Tectonophysics 792:228597

Kumar A, Srivastava P (2018) Landscape of the Indus river. The Indian Rivers: Scientific and Socio-economic Aspects 47–59

Kumar A, Devrani R, Srivastava AP (2022) Landscapes and paleoclimate of the Ladakh Himalaya. Advances in remote sensing technology and the three poles 308–320

Lakhan N, Singh AK et al (2019) Zircon U–Pb geochronology, mineral and whole-rock geochemistry of the Khardung volcanics, Ladakh Himalaya, India: Implications for Late Cretaceous to Palaeogene continental arc magmatism. Geol J. https://doi.org/10.1016/S0012-821X(99)00098-9

Lal R, Saini HS, Pant NC, Mujtaba SAI (2018) Tectonics induced switching of provenance during the Late Quaternary aggradation of the Indus River Valley, Ladakh. India Geosci Front 92:102–119

Lanci L, Hirt AM, Lowrie W, Lotter AF, Lemcke G, Sturm M (1999) Mineral-magnetic record of Late Quaternary climatic changes in a high Alpine lake. Earth Planet Sci Lett 170:49–59

Lascu I, Plank C (2013) A new dimension to sediment magnetism: charting the spatial variability of magnetic properties across lake basins. Global Planet Change 110:340–349

Laskar J, Robutel P, Joutel F, Gastineau M, Correia AC, Levrard B (2004) A long-term numerical solution for the insolation quantities of the Earth. Astron Astrophys 428(1):261–285

Li Y, Yu Z, Kodama KP, Moeller RE (2006) A 14,000-year environmental change history revealed by mineral-magnetic data from White Lake, northwestern New Jersey, USA. Earth Planet Sci Lett 246(1–2):27–40

Lisiecki LE, Raymo ME (2005) A Pliocene-Pleistocene stack of 57 globally distributed benthic D18O records. Palaeoceanogr 20(1):1003

Maher BA, Thompson R (1999) Quaternary environments, climates and magnetism. Cambridge University Press, pp 321–331 (**ISBN 978-0-521-62417-6**)

Maity M, Venkateshwarlu M, Mondal S, Kapawar MR, Gain D, Chatterjee S, Paul P (2022) Mineral magnetic and geochemical characterization of the dust and soils around Mejia Thermal Power Plant, West Bengal: Implications to source apportionment. J Earth Syst Sci 131:138

Mayewski PA, Jeschke PA (1979) Himalayan and Trans- Himalayan glacier fluctuations since AD 1812. Arct Alp Res 11(3):267–287

Mohamad AMO, Paleologos EK (2018) Magnetic Properties of Soils. Ed.: Fundamentals of Geoenvironmental Engineering: Understanding Soil, Water, and Pollutant Interaction and Transport. Butterworth-Heinemann, 535–580

Morthekai P, Nawaz AS (2014) Luminescence dating using Quartz for end-users. Gondwana Geol Mag 29:1–10

Mujtaba SAI, Lal R, Saini HS, Kumar P, Pant NC (2018) Formation and breaching of two paleolakes around Leh, Indus valley, during the late Quat. Geol Soc 462(1):23–34

Murray AS, Olley JM (2002) Precision and accuracy in the optically stimulated luminescence dating of sedimentary quartz: a status review. Geochronometria 21

Nag D, Phartiyal B (2015) Climatic variations and geomorphology of the Indus River valley, between Nimo and Batalik, Ladakh (NW trans Himalayas) during late quaternary. Quat Int 371:87–101

Nag D, Phartiyal B, Singh DS (2016) Sedimentary characteristics of paleolake deposits along the Indus River valley, Ladakh, Trans-Himalaya: implications for the depositional environment. Sedimentol 63:1765–1785

Nag D, Phartiyal B, Agrawal S, Kumar P, Sharma R, Kumar K, Joshi M (2023) Westerly-monsoon variations since the last deglaciation from semi-arid Ladakh region, Trans Himalaya, India. Palaeogeogr Palaeoclimatol Palaeoecol 618:111515

Owen LA (2011) Quaternary glaciation of northern India. Dev Quat Sci 15:929–942

Owen LA, Benn DI (2005) Equilibrium-line altitudes of the Last Glacial Maximum for the Himalaya and Tibet: an assessment and evaluation of results. Quat Int 138–139:55–78

Owen LA, Derbyshire E, Fort M (1998) The Quaternary glacial history of the Himalaya. Quat Proc 6:91–120

Owen LA, Caffee MW, Kelly RB, Finke RF, Milap CS (2006) Terrestrial cosmogenic nuclide surface exposure dating of the oldest glacial successions in the Himalayan Orogen: Ladakh Range, Northern India. Geol Soc Am Bull 118(34):383–392

Parés JM (2015) Sixty years of anisotropy of magnetic susceptibility in deformed sedimentary rocks. Front Earth Sci. https://doi.org/10.3389/feart.2015.00004

Parrenin F, Valerie MD, Peter K, Dominique R, Didier P, Jakob S, Carlo B, Amaelle L, Anna W, Jean J (2013) Antarctic Temperature Stack (ATS) from five different ice cores (EDC, Vostok, Dome Fuji, TALDICE, and EDML). Pangaea. https://doi.org/10.1594/PANGAEA.810188

Patel PP, Guha S, Das D, Bose M (2022) Spatial variability of topographic attributes and channel morphological characteristics in the Ladakh Trans-Himalayas and their tectonic and structural controls. In Himalayan Neotectonics and Channel Evolution 67–110

Petterson MG (2023) Structural Geology of the High Strain Zone: Ladakh Batholith, Leh Region, NW India. In: Himalayan Thick-Skin Basement Deformation of the Ladakh Batholith, Leh-Ladakh Region, NW India 65–100

Phartiyal B, Sharma A (2009) Soft-sediment deformation structures in the Late Quaternary sediments of Ladakh: evidence for multiple phases of seismic tremors in the North-western Himalayan Region. J Asian Earth Sci 34:761–770

Phartiyal B, Sharma A, Upadhyay R, Ram-Awatar A, Sinha AK (2005) Quaternary geology, tectonics and distribution of paleo- and present fluvio/glacio lacustrine deposits in Ladakh, NW Indian Himalaya-A study based on field observations. Geomorphology 65(3–4):241–256

Phartiyal B, Sharma A, Kothyari GC (2013) Damming of River Indus during Late Quaternary in Ladakh Region of Trans-Himalaya, NW India: implications to Lake formation-climate and tectonics. Chin Sci Bull 58(S1):142–155

Phartiyal B, Singh R, Kothrari GC (2015) Late Quaternary geomorphic scenario due to changing depositional regimes in the Tangtse Valley, Trans-Himalaya, NW India. Paleogeogr Paleoclimatol Paleoecol 422:11–24

Phartiyal B, Singh R, Nag D, Sharma A, Agnihotri R, Prasad V, Thakur B (2021) Reconstructing climate variability during the last four millennia from trans-Himalaya (Ladakh-Karakoram, India) using multiple proxies. Palaeogeogr Palaeoclimatol Palaeoecol 562:110142

Phartiyal B, Nag D, Joshi P (2022) Holocene climatic record of Ladakh, Trans-Himalaya. In Holocene Climate Change and Environment 61–89

Rhodes EJ (2011) Optically stimulated luminescence dating of sediments over the past 200,000 years. Annu Rev Earth Planet Sci 39:461–488

Rhodes EJ, Bailey RM (1997) The effect of thermal transfer on the zeroing of the luminescence of quartz from recent glaciofluvial sediments. Quat Sci Rev 16:291–298

Robertson, AHF, Collins AS (2002) Shyok Suture Zone, N Pakistan: late Mesozoic–Tertiary evolution of a critical suture separating the oceanic Ladakh Arc from the Asian continental margin. J Asian Earth Sci 20(3):309–351

Sangode SJ, Phadtare NR, Meshram DC, Rawat S, Suresh N (2011) A record of Lake Outburst in the Indus valley of Ladakh Himalaya, India. Curr Sci 100:1712–1718

Sangode SJ, Rawat S, Meshram DC, Phadtare NR, Suresh N (2013) Integrated mineral magnetic and lithologic studies to delineate dynamic modes of depositional conditions in the Leh valley basin, Ladakh Himalaya, India. J Geol Soc India 82(2):107–120

Sant DA, Wadhawan SK, Ganjoo RK, Basavaiah N, Sukumaran P, Bhattacharya S (2011a) Morphostratigraphy and paleoclimate appraisal of the Leh valley, Ladakh Himalayas, India. J Geol Soc India 77(6):499–510

Sant DA, Wadhawan SK, Ganjoo RK et al (2011b) Linkage of paraglacial processes from last glacial to recent inferred from Spituk sequence, Leh valley, Ladakh Himalaya. J Geol Soc India 78(2):147–156

Scharer U, Hamet J, Allegre CJ (1984) The Trans Himalaya (Gangdese) plutonism in the Ladakh region: a U-Pb and Rb–Sr study. Earth Planet Sci Lett 67:327–339

Scherrenberg M, Berends C, van de Wal R (2023) Late Pleistocene glacial terminations accelerated by proglacial lakes. Climate of the Past Discussions 1–30

Searle MP, Pickering KT, Cooper DJW (1990) Restoration and evolution of the intermontane Indus molasse basin, Ladakh Himalaya, India. Tectonophysics 174:301–314

Sharma MC, Chand P (2016) Studies on quaternary glaciations in India during 2010–2016. Proc Indian Nat Sci Acad 82:869–880

Sharma A, Phartiyal B (2018) Late quaternary paleoclimate and contemporary moisture source to extreme NW India: a review on present understanding and future perspectives. Front Earth Sci 6:150

Sharma CP, Chahal P, Kumar A, Singhal S, Sundriyal YP, Ziegler AD, Agnihotri R, Wasson RJ, Shukla UK, Srivastava P (2021) Late Pleistocene-Holocene flood history, flood-sediment provenance and human imprints from the upper Indus River catchment. Ladakh Himalaya GSA Bull 134(1–2):275–292

Sharma A, Phartiyal B (2020) Geomorphological changes during quaternary period vis a vis role of climate and tectonics in Ladakh, Trans-Himalaya. Himalayan Weather and Climate and their Impact on the Environment 159–183

Shukla UK, Kotlia BS, Mathur PD (2002) Sedimentation pattern in a trans-Himalayan Quaternary lake at Lamayuru (Ladakh), India. Sediment Geol 148(3–4):405–424

Shukla AD, Sharma S, Rana N, Bisht P, Juyal N (2020) Optical chronology and climatic implication of glacial advances from the southern Ladakh Range, NW Himalaya, India. Palaeogeogr Palaeoclimatol Palaeoecol. 539:109505

Sinclair HD, Jaffey N (2001) Sedimentology of the Indus Group, Ladakh, northern India: implications for the timing of initiation of the palaeo-Indus River. J Geol Soci 158(1):151–162

Srivastava P, Ray Y, Phartiyal B et al (2013) Late Pleistocene-Holocene Morphosedimentary architecture, Spiti River, Arid Higher Himalaya. Int J Earth Sci 102:1967–1984

The Rock Color Chart Committee (1980) Rock Color Chart. Geol. Society of America, Boulder USA. https://munsell.com/about-munsell-color/. Accessed 10–010–2023

Thouveny N, Debeaulieu JL, Bonifay E, Creer KM et al (1994) Climate variations in Europe over the past 140-kyr deduced from rock magnetism. Nature 371:503–506

Tweed FS, Carrivick JL (2015) Deglaciation and proglacial lakes. Geol Today 31(3):96–102

Upadhyay R, Frisch W, Siebel W (2008) Tectonic implications of new U-Pb zircon ages of the Ladakh batholith, Indus suture zone, northwest Himalaya, India. Terra Nova 20(4):309–317

Vergnano A, Oggeri C, Godio A (2023) Geophysical-geotechnical methodology for assessing the spatial distribution of glacio-lacustrine sediments: the case history of Lake Seracchi. Earth Surf Proc Landforms 48(7):1374–1397

Verosub KL, Roberts AP (1995) Environmental magnetism: past, present and future. J Geophys Res 100(B2):2175–2192

Vlag P, Thouveny N, Williamson D, Andrieu V, Icolel M, Van Velzen AJ (1997) The rock magnetic signal of climate change in the maar lake sequence of Lac St Front (France). Geophys J Int 131:724–740

Wallinga J (2002) On the detection of OSL age overestimation using single-aliquot techniques. Geochronometria 21

Wang X, Yang Z, Løvlie R, Min L (2004) High-resolution magnetic stratigraphy of fluvio-lacustrine succession in the Nihewan Basin. China Quat Sci Rev 23(9–10):1187–1198

Ye C, Yang Y, Fang X, Zan J, Tan M, Yang R (2020) Chlorite weathering linked to magnetic enhancement in Red Clay on the Chinese Loess Plateau. Paleogeogr Paleoclimatol Paleoecol 538:109446

Yin Y, Fang NQ, Wang Q, Nie HG, Qing ZL (2002) Magnetic susceptibility of lacustrine sediments and its environmental significance: evidence from Napahai lake, northwestern Yunnan. China Scientia Geographica Sinica/dili Kexue 22(4):413–419

Zhou R, Aitchison JC, Lokho K, Sobel ER, Feng Y, Zhao J (2020) Unroofing the Ladakh Batholith: constraints from autochthonous molasse of the Indus Basin, NW Himalaya. J Geol Soc 177(4):818–825

Ziegler AD, Cantarero SI, Wasson RJ, Srivastava P, Spalzin S, Chow WT, Gillen J (2016) A clear and present danger: Ladakh's increasing vulnerability to flash floods and debris flows. Hydrol Proces 30(22):4214–4223